Quaternary Science Reviews 222 (2019) 105903

Contents lists available at ScienceDirect

Quaternary Science Reviews

journal homepage: www.elsevier.com/locate/quascirev

Abrupt shifts of productivity and sea ice regimes at the western Barents Sea slope from the Last Glacial Maximum to the Bølling-Allerød interstadial

Denizcan Köseoğlu [a, *], Simon T. Belt [a], Jochen Knies [b, c]

[a] Biogeochemistry Research Centre, School of Geography, Earth and Environmental Sciences, Plymouth University, Plymouth, PL4 8AA, UK
[b] CAGE – Centre for Arctic Gas Hydrate, Environment and Climate, Department of Geosciences, UiT The Arctic University of Norway, 9037 Tromsø, Norway
[c] Geological Survey of Norway, N-7491 Trondheim, Norway

ARTICLE INFO

Article history:
Received 30 April 2019
Received in revised form
27 August 2019
Accepted 27 August 2019
Available online 12 September 2019

Keywords:
Arctic Ocean
Quaternary
Sea ice
Marine biomarkers
HBI
IP_{25}
PIP_{25}
Barents Sea
Coastal polynya
Classification tree

ABSTRACT

Advanced knowledge of spatio-temporal constraints on the Barents Sea Ice Sheet during the late Weichselian glaciation overshadows relatively limited understanding of seasonal sea ice (experiencing an annual advance-retreat cycle) and primary productivity trends accompanying massive, abrupt climate changes during glacial-deglacial cycles. Such paleo-reconstructions are crucial prerequisites for improved comprehension and prediction of current and future climate change. Here, we investigate sea ice and phytoplankton biomarker distributions in a Barents Sea sediment core covering ca. 25.8–15.4 cal kyr BP to elucidate abrupt shifts of spring–summer sea ice concentrations and relative sympagic–pelagic productivity trends at the southwestern continental slope. Despite significant presence of seasonal sea ice, the Last Glacial Maximum (LGM) and initial shelf edge deglaciation (SEDG) at the core site are characterised by occurrence of productive coastal polynya adjacent to the maximum ice sheet extent. The onset of perennial (i.e. multi-year) ice cover and near-zero productivity during Heinrich Stadial 1 (HS1; ca. 18.0–16.3 cal kyr BP) accompanies significant meltwater fluxes from ice sheet debuttressing and the consequent stagnation of thermohaline circulation. Rapid sea ice retreat and unprecedented pelagic productivity observed after 16.3 cal kyr BP coincides with areal ice sheet deglaciation and is potentially linked to the release of sub-surface heat and nutrient reservoirs, together with reinvigorated deep water circulation following millennial heating of the deep ocean during HS1. We find that a multivariate fingerprinting approach involving assessment of both downcore and surface biomarker distributions is able to distinguish relative ice-algal and pelagic diatom productivity driven by sea ice dynamics.
© 2019 Elsevier Ltd. All rights reserved.

1. Introduction

Arctic sea ice cover is an integral component of the climate system and exhibits complex interactions with the ocean and the atmosphere. High albedo allows sea ice to effectively reflect incoming solar radiation during the spring and summer months, while extensive areal coverage during winter prevents excessive oceanic heat loss, thus regulating the heat budget across the ocean-atmosphere interface (e.g. Smedsrud et al., 2013). Oceanic convection from brine expulsion during ice formation contributes to the thermohaline overturning circulation (Berger and Jansen, 1995), while occurrence of leads, polynya and seasonal ice melting stratifies the water column, facilitating between 10 and 55% of all primary productivity in the Arctic Ocean (Gosselin et al., 1997; Wassmann et al., 1999, 2006). The decline of seasonal sea ice extent (Fetterer et al., 2017), thickness (Lindsay and Schweiger, 2015), and perennial (multi-year) ice fraction (Smedsrud et al., 2017) evident since ca. 1850 AD (Walsh et al., 2017) has accelerated further over the last ca. 40 years. Such a precipitous decline is augmented via positive feedback (Smedsrud et al., 2013) and is likely caused by a combination of anthropogenic warming (Notz and Marotzke, 2012), as well as increasing inflow and temperature of Atlantic Water (AW) (Årthun et al., 2012). The latter is most evident in the seasonally ice-covered Barents Sea, where the North Atlantic Current (NAC) provides ample nutrients for spring-summer primary productivity blooms (e.g. Wassmann et al., 1999,

* Corresponding author.
E-mail addresses: deniz.koseoglu@plymouth.ac.uk, denizcan.koseoglu@gmail.com (D. Köseoğlu).

https://doi.org/10.1016/j.quascirev.2019.105903
0277-3791/© 2019 Elsevier Ltd. All rights reserved.

2006). Higher volume and temperature of AW and multi-decadal recession of the Barents Sea ice cover (Onarheim et al., 2018) are already contributing to earlier ice melt, increased lead/polynya incidence (Willmes and Heinemann, 2016), hastening of spring phytoplankton blooms (Stroeve et al., 2014), and northward intrusion of lower-energy, smaller pelagic species at the expense of ice-obligate algae (Hegseth and Sundfjord, 2008; Assmy et al., 2017; Hoppe et al., 2018) that likely affects survivability and biodiversity of pelagic and benthic communities in the region (Søreide et al., 2013). The motivation of understanding such implications and forecasting development of high-latitude oceans in a warming climate implies paleo-reconstruction of sea ice conditions and associated responses of sympagic and pelagic biota over longer timescales.

Such paleo reconstructions can potentially be obtained through the analysis of proxy measures of sympagic and pelagic primary production in sedimentary records whose temporal coverage includes significant shifts in oceanographic and sea ice conditions. Sea ice reconstructions traditionally involve analysis of census data and isotopic composition of calcareous and siliceous microfossils, including foraminifer tests, dinocysts and diatom frustules (De Vernal et al., 2013, and references therein). However, microfossils are susceptible to carbonate and silicate dissolution in corrosive waters formed, for example, via brine rejection during ice formation (Zamelczyk et al., 2014). Such challenges may potentially be circumvented via analysis of certain geochemical lipid biomarkers, such as highly-branched isoprenoids (HBIs; Belt and Müller, 2013; Belt, 2018) and sterols (Volkman, 1986), which are often more stable over geologically-significant timescales (e.g. Stein and Fahl, 2013) and can be source-specific (Belt and Müller, 2013; Belt, 2018). A suite of such biomarker proxies representing contrasting primary production sources (e.g. sympagic versus pelagic) may therefore be used to reconstruct environmental variability over temporal windows spanning significant climate shifts. For example, the LGM in the Barents Sea between ca. 26.5–19.0 cal kyr BP (Clark et al., 2009; Peltier and Fairbanks, 2006) and eventual collapse of the Barents Sea Ice Sheet (BSIS) between ca. 18.0–17.5 cal kyr BP (Bauch et al., 2001; Dokken and Jansen, 1999; Elverhøi et al., 1995; Knies et al., 2018) are relevant time intervals for investigating the interactions between AW inflow, Atlantic Meridional Overturning Circulation (AMOC), sea ice concentration, and primary productivity. Geochemical evidence suggests that the LGM and post-deglaciation intervals exhibited heavy seasonal sea ice and near ice-free conditions, respectively, and were punctuated by the Heinrich Stadial 1 (HS1), when harsh glaciomarine conditions and weakened AW inflow prevented growth of biota (e.g. Jennings et al., 2018; Knies et al., 2018; Müller et al., 2009; Müller and Stein, 2014). Such contrasting conditions that characterised these time intervals, coupled with the direct interaction of AW inflow with both the maximum-extent BSIS and the adjacent sea ice margin, make the Late Weichselian Barents Sea key for elucidating the interactions between oceanographic conditions, the sea ice regime, and the associated interplay of sympagic and pelagic primary productivity. Such an investigation could also aid the understanding of potential consequences associated with the projected debuttressing of the contemporary West Antarctic Ice Sheet (WAIS) (Hulbe, 2017), for which the Late Weichselian BSIS was previously suggested as a close paleo-analogue (Andreassen and Winsborrow, 2009; Bjarnadóttir et al., 2014).

The focus of this study was, therefore, to reconstruct sea ice conditions and associated changes in primary productivity at the western Barents Sea continental slope throughout extreme climate shifts spanning ca. 25.8–15.4 cal kyr BP. To achieve this, we quantified a multivariate set of 10 geochemical biomarkers (Table 1) representing ice-algal and marine phytoplankton input (Fig. 1) in a marine sediment core (Fig. 2b) to assess the roles of ice cover and coastal polynya proximal to the BSIS in sustaining both sympagic and pelagic primary productivity from the LGM to the retreat of sea ice cover preceding the Bølling-Allerød (BA) interstadial. Downcore biomarker distributions were compared to those of proximal surface sediments to identify paleo-analogues of contemporary sea ice and productivity settings or, alternatively, determine whether certain intervals within the downcore record represent unique conditions not reproduced in the current climate.

2. Biomarker background

HBIs are unsaturated hydrocarbons produced exclusively by a relatively narrow range of marine and lacustrine diatoms (Belt and Müller, 2013; Belt, 2018). A C_{25} HBI discovered in Canadian Arctic sea ice and labelled IP_{25} (Belt et al., 2007) was confirmed as a seasonal sea ice proxy due to its accumulation during the spring diatom bloom in March–April (Brown et al., 2011) and Arctic sea ice diatom sources (*Pleurosigma* and *Haslea* spp.; Brown et al., 2014b), all of which also contribute to Barents Sea spring blooms (Von Quillfeldt, 2000). Notably, at least certain productive sea-ice diatom species abundant in multi-year ice (Syvertsen, 1991; Boetius et al., 2013), such as *Melosira arctica*, do not produce IP_{25} or any other HBIs. Accordingly, numerous analyses of surface sediments ($n > 850$) spanning the Arctic Ocean showed near-ubiquitous presence of IP_{25} in seasonally ice-covered locations, and either very low abundance or absence in regions of year-round open water or multi-year ice cover, such as that found in the central Arctic (Xiao et al., 2013). IP_{25} has since been extensively used for reconstructing past sea ice variability throughout the Arctic Ocean and the Nordic Seas (Belt, 2018, and references therein). An HBI diene (HBI II; Table 1) is co-produced (Brown et al., 2014b) and usually highly correlated (e.g. Cabedo-Sanz et al., 2013; Xiao et al., 2013) with IP_{25}. The latter is often combined with a marine phytoplankton biomarker (e.g. brassicasterol, dinosterol; Volkman, 1986) into the Phytoplankton–IP_{25} index (PIP_{25}; Eq. (1) and Fig. 1) to obtain semi-quantitative descriptions of sea ice conditions (e.g. Müller et al., 2011; Stein et al., 2017; Xiao et al., 2015). More recently, the calculation of a $P_{III}IP_{25}$ index using a tri-unsaturated HBI (HBI III; Table 1 and Fig. 1) as the phytoplankton biomarker resulted in semi-quantitative spring sea ice concentration (SpSIC) estimates in the Barents Sea (Belt et al., 2015; Berben et al., 2017; Smik et al., 2016). Further, HBI III and its diastereoisomer (HBI IV; Table 1 and Fig. 1) were recently detected in the pelagic diatom *Rhizosolenia setigera* near Western Svalbard (Belt et al., 2017). Indeed, *R. setigera* is likely the most cosmopolitan among identified producers of trienes III and IV (Belt et al., 2000; Brown et al., 2014a), given its identification as one of most globally abundant diatoms (Leblanc et al., 2012) and the capacity of certain *Rhizosolenia* spp. for active buoyancy control (Joseph et al., 1997) and formation of macroscopic mats under nutrient-replete conditions (Yoder et al., 1994). Together with high correlation and clear enhancement of both biomarkers near the receding spring sea ice edge (Belt et al., 2015), this supports the use of HBIs III and IV as indicators of pelagic diatom productivity in the Barents Sea. Thus, the availability of a multivariate HBI biomarker set in Barents Sea surface sediments (IP_{25}, HBIs II, III and IV; Table 1 and Fig. 1) recently prompted the development of a classification tree (CT) model of HBI distributions (Fig. 1) in surface sediments as a viable method of categorising sea ice conditions over centennial to millennial timescales (Köseoğlu et al., 2018a, 2018b). These investigations showed clear enhancement of pelagic HBIs III and IV relative to sympagic IP_{25} and HBI II in the productive Barents Sea MIZ, while the reverse was evident under heavy ice cover northeast off Svalbard. The database of HBI concentrations in Barents Sea surface sediments therefore provides

Table 1
Uses and potential limitations of HBI and sterol lipids utilised as biomarkers of sea ice and primary productivity regimes in the current study. Relevant citations are represented by superscripted numbering.

Lipid biomarkers	Common use(s)	Potential limitation(s)	Present interpretation	References
HBIs				
IP_{25} and II	Source-specific, co-produced diatom proxies of seasonal Arctic sea ice[1, 2]. Stable within sedimentary record and resistant to photodegradation and autoxidation[3].	Require concurrent analysis of an open-water biomarker(s) to distinguish perennial ice and open water settings[4, 5, 6, 7]. Only represent productivity of minor sympagic diatoms[1, 2].	Used as indicators of sympagic diatom productivity within sea ice, where absolute concentrations and relative abundances increase with longer seasonal sea ice duration.	Belt et al. (2015[5], 2016[2], 2017[9]) Brown et al. (2014b)[1] Köseoğlu et al. (2018a,b)[7] Müller et al. (2011)[4] Ringrose (2012)[8] Rontani et al. (2011, 2014b)[3] Smik et al. (2016)[6]
III and IV	Ubiquitous pelagic diatom proxies vastly enhanced during the spring MIZ phytoplankton bloom, and limited under extensive ice conditions[5, 6, 7]. III used to derive $P_{III}IP_{25}$-based SpSIC estimates[5, 6], and IV used for CT predictions of sea ice cover[7].	Increased degradation rates relative to IP_{25} and II, at least under laboratory conditions[3]. IV (<10%) detected in sea ice, while all but one *in-situ* sources in the Arctic (*Rhizosolenia setigera*) are still unknown[9].	Used as indicators of pelagic diatom productivity in the photic zone of the water column. Absolute concentrations and relative abundances increase under highly-productive conditions.	**Reviews:** Belt and Müller (2013) Belt (2018)
Sterols				
Brassicasterol	A major constituent of marine algae and indicative of general productivity[10].	Present in sea ice[11].	Due to their reduced source-specificity, variability of all absolute sterol concentrations was interpreted as a general indicator of changes in marine productivity. Comparison of sterol relative abundance distributions downcore to those of surface sediments was used to identify similarities and differences between paleo and more recent/ contemporary settings characterised by contrasting sea ice and/or productivity conditions.	Belt et al. (2013, 2018)[11] Boon et al. (1979)[15] Hassett and Crockett (2009)[19] Huang and Meinschein (1976)[14] Mühlebach et al. (1999)[18] Nichols et al. (1990)[16] Rampen et al. (2010)[10] Rontani et al. (2014a, 2016)[12] Volkman et al. (1993)[17] **Review:** Volkman (1986)[13]
Chalinasterol	An indicator of marine diatom productivity as the dominant sterol in many centric and pennate diatoms[10].	Susceptible to photodegradation and autoxidation[12]; Found in other algae (e.g. cryptomonads), and in sea ice[11, 13].		
Campesterol and β-sitosterol	Commonly associated with terrigenous input from vascular plants[14].	Found in many diatoms, where β-sitosterol often dominates the sterol assemblage[10].		
Dinosterol	A common biomarker of dinoflagellate productivity[15].	Detected as a minor constituent of diatoms (including sympagic) in polar settings[16] and cultures[17].		
Cholesterol	High proportional abundance can indicate increased marine faunal productivity[13].	Ubiquitous amongst vertebrates[18, 19] and diatoms[10].		

an opportunity to determine whether, and to what extent, HBI distributions characteristic of different sea ice regimes in the modern Barents Sea are reproduced within the Late Weichselian sedimentary sequence.

To complement the HBI data, we also analysed several sterol lipids, which are ubiquitous components of eukaryotes (Volkman, 1986). In marine settings, the particular diversity of C_{27}–C_{29} sterols among microorganisms, including microalgae and plankton (Volkman, 2003), has facilitated their use as chemotaxonomic biomarkers of organic matter sources in paleo-environments, including high-latitude shelf seas (e.g. Belt et al., 2013; Knies, 2005). Despite this, few sterols are considered unambiguous biomarkers of specific algal groups as many classes of marine microorganisms contribute the same sterols to the sedimentary budget (Volkman, 1986). For instance, 24-methylcholesta-5,22*E*-dien-3β-ol (epibrassicasterol) and 24-methylcholesta-5,24(28)-dien-3β-ol (24-methylenecholesterol or chalinasterol) are often used as indicators of diatom primary production, despite the fact that the former is often not a major constituent of diatoms (Rampen et al., 2010) and is found in other clades of algae (Volkman, 1986; Volkman et al., 1999). Additionally, epibrassicasterol has been utilised as an indicator of pelagic phytoplankton productivity in ice-covered regions (e.g. Navarro-Rodriguez et al., 2013), in spite of its abundance in sea ice (Belt et al., 2013, 2018) and pennate diatoms (e.g. Rampen et al., 2010). Moreover, diatoms often produce C_{29} sterols (Belt et al., 2013, 2018; Rampen et al., 2010), such as 24-ethylcholest-5-en-3β-ol (β-sitosterol) and 24-methylcholest-5-en-3β-ol (campesterol) traditionally associated with vascular plants (Huang and Meinschein, 1976), which makes distinguishing between marine and terrigenous organic matter in sediments challenging. Even 4-methyl C_{30} sterols, such as 4α,23,24-trimethyl-5α-cholesta-22-en-3β-ol (dinosterol), traditionally considered to be exclusive to dinoflagellates (Boon et al., 1979) and more specific to marine productivity (e.g. Knies, 2005), have been detected in both sea ice (Nichols et al., 1990) and diatom cultures (*Navicula* spp.; Volkman et al., 1993). Such factors underline the need to consider more source-specific biomarkers, such as HBIs representative of sympagic and pelagic sources, in addition to sterols when decoupling ice-covered and open water conditions in paleo-records (Belt et al., 2015; Smik et al., 2016). Despite their wide distribution across different biota, sterols remain useful indicators of both marine and terrigenous sedimentation, as well as general marine primary productivity, provided such inferences are drawn from a multivariate sterol record further contextualised using other proxy data (Volkman, 1986) or more source-specific biomarkers ,such as IP_{25} and other HBIs. Here, we focus on downcore relative abundance distributions of a multivariate sterol set (Table 1), and compare these with surface sediment sterol distributions representative of contrasting sea ice and productivity conditions in the modern Barents and Norwegian seas.

3. Modern regional setting

The warm and saline NAC carries a significant amount of heat into the seasonally ice-covered Barents Sea (Smedsrud et al., 2010), which continues along the western and northern continental

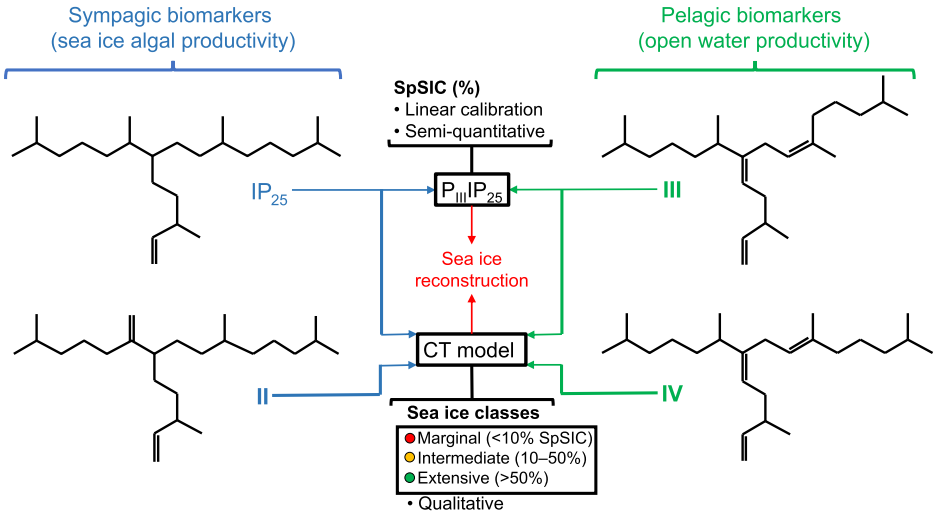


Fig. 1. Structures of IP_{25} and HBI II (representing sea ice diatom productivity), as well as HBIs III and IV (indicative of pelagic diatom productivity). The combined use of HBIs within proxies for sea ice reconstruction (including $P_{III}IP_{25}$ and CT models) is illustrated.

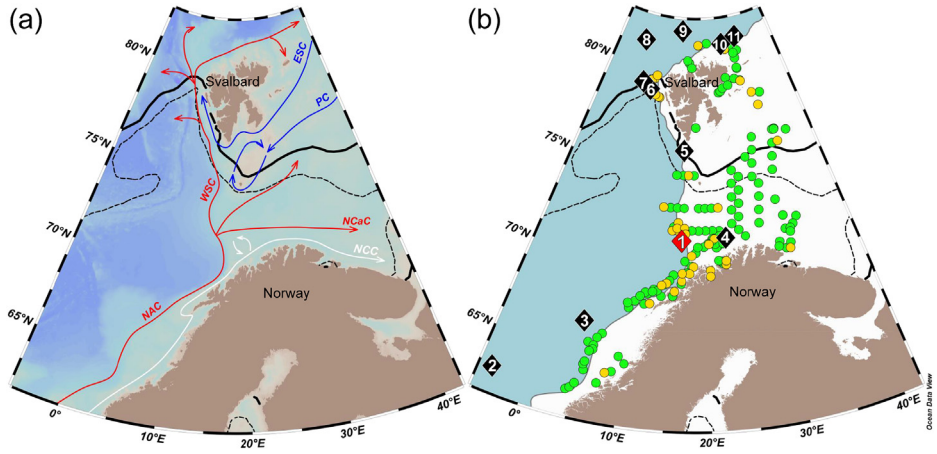


Fig. 2. Maps of the Barents Sea showing: (a) The main inflow currents carrying AW (via the NAC, NCaC, and WSC), ArW (PC and ESC), and CW (NCC); (b) Surface and downcore sample locations. Green and orange circles correspond to surface sediment locations where HBI with or without additional sterol data were available for comparison with downcore records, respectively. Both the investigated site and referenced downcore locations are shown by numbered diamond markers: (1) GS14-190-PC01 (this study and Knies et al., 2018); (2) JM11-F1-19PC (Hoff et al., 2016); (3) MD95-2010 (Marcott et al., 2011); (4) JM05-85-GC (Aagaard-Sørensen et al., 2010); (5) JM02-460 GC/PC (Rasmussen et al., 2007); (6) MSM5/5-712-2 (Müller and Stein, 2014); (7) PS93/006-1 (Kremer et al., 2018a); (8) PS2837-5 (Wollenburg et al., 2004; Müller et al., 2009); (9) PS92/039-2 (Kremer et al., 2018b); (10) HH11-09GC (Chauhan et al., 2016); (11) PS2138-1 (e.g. Knies and Stein, 1998; Nørgaard-Pedersen et al., 2003). Maximum BSIS extent throughout the LGM (at ca. 21 cal kyr BP) is shown by a filled white area (Hughes et al., 2016). In both maps, dashed and solid black lines correspond to averaged SpSIC contours (April–June; 1988–2017) of 0% and 15%, respectively. (For interpretation of the references to colour in this figure legend, the reader is referred to the Web version of this article.)

margins as the largely sub-surface West Spitsbergen Current (WSC), while the North Cape Current (NCaC) branches out towards Novaya Zemlya and the central Barents Sea (Fig. 2a). Fresher coastal water (CW) from the Baltic Sea flows inshore of the NAC with the Norwegian Coastal Current (NCC). Southwest-bound Arctic Water (ArW) enters the Barents Sea with the East Spitsbergen and Persey Currents (ESC and PC, respectively), forming a fresher and colder surface layer around Svalbard (Loeng, 1991; Smedsrud et al., 2013). Effective turbulent mixing of warm AW towards the surface during the winter (October–March), when over half of the Barents Sea may be ice-covered (Fetterer et al., 2017), facilitates selective thinning of the ice cover along the path of inflowing AW and keeps a significant portion of western and northern Svalbard shelves ice-free (Ivanov et al., 2012). Ice recession towards the northern shelf break occurs throughout the insolation-triggered melt season during spring and summer (April–September). The interplay of freshwater input and increased light penetration due to melting sea ice stabilises free-floating phytoplankton and AW-carried nutrients within the euphotic zone, developing extensive, but short-lived primary productivity blooms in the MIZ around the retreating ice margin (Wassmann et al., 1999, 2006). The resulting algal biomass fuels energy transfer to higher trophic levels (e.g. zooplankton) and eventually reaches the ocean floor, helping sustain benthic life (Søreide et al., 2013). Further, the development of leads and polynyas coupled with weak stratification from AW-induced melting of sea ice may trigger under-ice pelagic blooms even prior to the melt season (Assmy et al., 2017; Strass and Nöthig, 1996). Sympagic blooms of ice algae develop up to two months prior to seasonal ice retreat as they do not rely on stratification and are triggered by increasing solar insolation in March (Signorini and McClain, 2009). Increasing temperature and volume of inflowing AW has already increased primary productivity by ca. 30% since the 1990's by

reducing sea ice extent and expanding that of the MIZ, prolonging and hastening the bloom season (Arrigo and van Dijken, 2015; Strong and Rigor, 2013). Nonetheless, average phytoplankton biomass at peak bloom is decreasing due to accelerated zooplankton grazing in a warming Barents Sea (Kvile et al., 2016).

4. Materials and methods

4.1. Sediment material

The 1384 cm long GS14-190-PC01 piston core (71.475° N, 16.165°E; 949 m water depth), hereafter GS14, was recovered aboard the RV "G.O. Sars" on June 3rd, 2014 at the southwestern Barents Sea slope (Fig. 2b). A detailed core chronology for the upper 694 cm of the core is available from Knies et al. (2018) and is based on six accelerator mass spectrometry (AMS) ^{14}C measurements of planktonic and benthic microfossils, including foraminifera and *Thyasira* spp. bivalves. This is supported by an additional six radiocarbon dates transferred to a common depth scale from the gravity core 33-GC08 (hereafter GC08) sampled from the same location as core GS14 using five tie-points inferred from XRF Ca records. The radiocarbon ages were calibrated to calendar ages (cal kyr BP) using the Marine13 curve (Reimer et al., 2013), and no local reservoir age correction was applied ($\Delta R = 0$). Finally, Bayesian accumulation age-depth modelling (Bacon 2.2) was used to create the age model (Blaauw and Christen, 2011).

In this study, core depths of 11.5–523 cm (ca. 25.8–15.4 cal kyr BP) were investigated, with the age model supported by four and five ^{14}C AMS dates from cores GS14 and GC08, respectively (Figs. 3–5). A total of 131 one centimetre sediment horizons were sampled with 10 mL cut-barrel plastic syringes, freeze-dried for 24–48 h (1 μbar; −80 °C) and frozen in plastic bags at −20 °C to preserve sample integrity prior to lipid extraction. While HBIs were extracted and analysed for all 131 horizons, sterol analysis was carried out separately using the same depth interval, but a lower sampling frequency (87 horizons) due to limited availability of material. Sedimentation rates ranged from 12.4 cm kyr^{-1} to 148.9 cm kyr^{-1} (Knies et al., 2018), resulting in a mean temporal resolution between analysed horizons of 81 ± 62 yr for HBIs and 115 ± 74 yr for sterols.

To supplement the GS14 downcore analysis, Barents and Norwegian Sea surface sediments ($n = 144$; Fig. 2b) representing contrasting contemporary sea ice conditions, and for a larger set of which ($n = 198$) HBI data was recently reported (Köseoğlu et al., 2018a), were re-extracted to obtain sterol distributions. Barents and Norwegian Seas were delineated using the International Council for the Exploration of the Sea (ICES) Ecoregions shapefiles (http://gis.ices.dk/geonetwork/srv/metadata/4745e824-a612-4a1f-bc56-b540772166eb). Surface and downcore absolute biomarker concentrations (ng g^{-1} dry sed.), downcore calibrated horizon ages (cal yr BP), and associated depths (cm) are available from Mendeley Data (doi: https://doi.org/10.17632/jx97c9nv3k.1).

4.2. Lipid extraction and analysis

HBIs were extracted according to the methods of Belt et al. (2012), with certain modifications. Briefly, an internal standard (9-octylheptadec-8-ene; 0.1 μg) was added to freeze-dried and homogenized sediment (ca. 2 g), and the total organic extract (TOE) was obtained following repeated sonication and centrifugation with a DCM: MeOH solvent mixture (2:1 v/v; 3 × 2 mL). The solvent was evaporated to dryness at 25 °C under N_2, and the TOE was re-suspended in hexane (ca. 1 mL). Elemental sulphur was removed by repeatedly shaking the sample with ca. 1 mL of tetrabutylammonium sulphite reagent (3.39 g in 100 mL of milliQ water saturated with 25 g of anhydrous sodium sulphite) and 2 mL of isopropanol, followed by decanting the supernatant hexane layer into a separate vial (4 × 1 mL). The partially purified extracts were evaporated to dryness (N_2; 25 °C), re-suspended in hexane (1 mL) and transferred onto hexane-conditioned chromatography columns (3 × 1 mL of hexane; ca. 1 g of 60–200 μm silica). A hydrocarbon fraction containing HBIs was eluted via hexane (ca. 7 mL), which was evaporated to dryness under N_2, re-suspended in hexane (ca. 300 μL) and further fractionated into saturated and unsaturated hydrocarbons on Ag-ion chromatography columns (Discovery® Ag-Ion; ca. 0.1 g) by successive elution with hexane (ca. 1 mL) and acetone (ca. 2 mL), respectively. The HBI-containing acetone fractions were evaporated to dryness and transferred to gas chromatographic (GC) vials (300 μL) in hexane.

Sterols were extracted following internal standard addition to sediments (5α-androstan-3β-ol; 0.1 μg) and saponification with 5% (m/v) methanolic potassium hydroxide (KOH; 9:1 v/v MeOH: milliQ water; 70 °C for 60 min). Impurities were partially removed by elution via 7:3 DCM: hexane (6 mL) on silica chromatography columns (ca. 1 g of hexane-conditioned silica) and sterols were subsequently collected using 4:1 (v/v) hexane: methyl acetate (ca. 7 mL). Following N_2 blowdown (25 °C), sterol-containing fractions were derivatised with N,O-bis(trimethylsilyl)trifluoroacetamide (BSTFA; 100 μL; 70 °C for 60 min) and transferred to GC vials (300 μL) in DCM.

Analysis of HBIs and sterols was carried out via gas chromatography–mass spectrometry (GC–MS) using established methods (Belt et al., 2012, 2013) with an Agilent 7890 gas chromatograph equipped with the HP_{5MS} fused-silica column (30 m; 0.25 μm film thickness; 0.25 mm internal diameter) coupled to an Agilent 5975 series mass spectrometric detector. All biomarkers were identified in total ion current (TIC) mode by comparison of peak retention indices ($RI_{HP5\text{-}MS} = 2081$ for IP_{25}, 2082 for HBI II, 2044 for HBI III and 2091 for HBI IV) (Belt, 2018, and references therein) and mass spectra to authentic standards and, in the case of sterols, to published data (Boon et al., 1979; Combaut, 1986). Quantification was carried out in selected ion monitoring (SIM) and TIC modes for HBIs and sterols, respectively. The resulting peak areas were corrected according to internal standard responses, instrumental response factors (RFs), and sediment mass. Re-calibration of RF values allowed us to quantify additional sterols, updating and extending the GS14 dinosterol record of Knies et al. (2018).

4.3. Statistical analysis

We used divisive changepoint analysis from the R package ECP (James and Matteson, 2013; R Core Team, 2018) on individual biomarker timeseries to identify significant shifts ($p = 0.005$) in biomarker profiles within the investigated temporal window (Figs. 3 and 4). $P_{III}IP_{25}$ values for each horizon were derived using a regional concentration balance factor for the Barents Sea (*c*-factor = 0.63; Eq. (1)) with non-zero absolute concentrations (ng g^{-1} dry sed., shown in square brackets in all equations) of IP_{25} and HBI III. Semi-quantitative estimates of spring sea ice concentrations (SpSIC, %; April–June) were subsequently calculated using the Barents Sea SpSIC–$P_{III}IP_{25}$ calibration (Eq. (2)) of Smik et al. (2016). The occurrence of summer sea ice (SuSIC, %; July–September) was tentatively inferred using a $P_{III}IP_{25}$-based SpSIC threshold of ca. 70% ($P_{III}IP_{25}$>0.8; Smik et al., 2016). Semi-quantitative SpSIC estimates were supplemented with categorical classification of each horizon into marginal (near ice-free waters; <10% SpSIC), intermediate (MIZ conditions with ca. 10–50% SpSIC), and extensive (heavy ice cover characteristic of north-eastern Svalbard; >50% SpSIC) sea ice conditions using the multivariate CT model of Köseoğlu et al. (2018a).

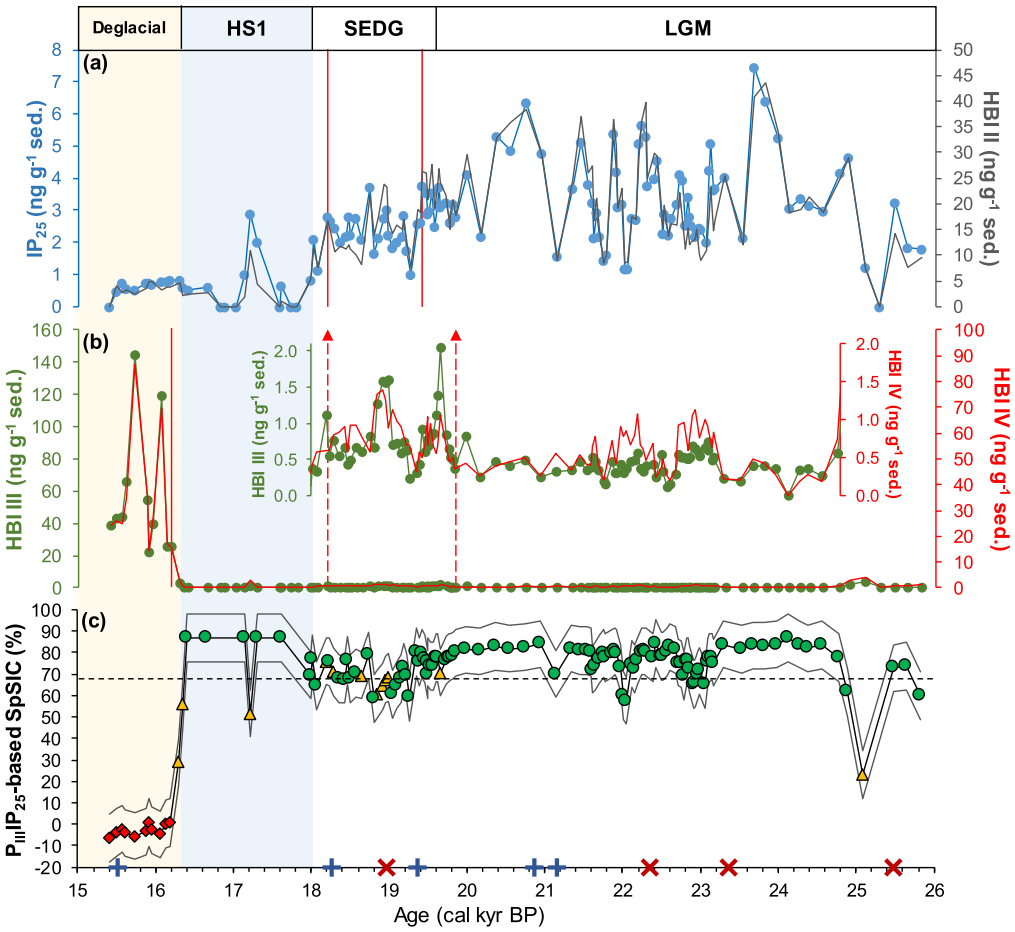


Fig. 3. HBI concentration profiles for core GS14: (a) IP_{25} and HBI II, indicative of sympagic diatom productivity; (b) HBIs III and IV, showing pelagic diatom productivity. A zoomed-in version of the profile spanning ca. 25–18 cal kyr BP is also shown; (c) $P_{III}IP_{25}$-based SpSIC (%) estimates with confidence limits (grey lines) corresponding to the standard error of calibration (ca. ±11%; Smik et al., 2016), and superimposed categorical CT predictions of marginal (ca. <10% SpSIC), intermediate (ca. 10–50% SpSIC), and extensive (>50% SpSIC) sea ice regimes denoted by red diamonds, yellow triangles, and green circles, respectively. The threshold for summer sea ice occurrence is shown by the horizontal dashed line. In all plots, coloured background bands constrain the LGM and SEDG (25.8–18.0 cal kyr BP), HS1 (18.0–16.3 cal kyr BP) and Deglacial (after 16.3 cal kyr BP) intervals – a rationale for dividing the GS14 record into time slices is provided in the Discussion. Changepoints significant at a 99.5% confidence level ($p < 0.005$) are shown by vertical red lines, where upward-pointing dashed arrows apply to the left y-axis only, while a solid line applies to both the left and right y-axes. Red and blue crosses highlight GS14 and GC08 ^{14}C AMS dates on the age scale, respectively. (For interpretation of the references to colour in this figure legend, the reader is referred to the Web version of this article.)

CT predictions were derived from percentage contributions of each HBI (IP_{25}, HBIs II, III and IV) to the total (Eq. (3)) and were not carried out for samples where no HBIs were detected.

$$P_{III}IP_{25} = \frac{[IP_{25}]}{([IP_{25}] + [III] \times 0.63)} \quad (1)$$

$$SpSIC\ (\%) = \frac{(P_{III}IP_{25} - 0.0692)}{0.0107} \quad (2)$$

$$HBI\ (\%) = \frac{[HBI]}{\sum([IP_{25}], [II], [III], [IV])} \times 100 \quad (3)$$

In addition to examining downcore profiles (Figs. 3 and 4), the absolute concentration (ng g^{-1} sed.) and compositional distributions (%; Eq. (3)) of all biomarkers were examined to identify significant distributional shifts and further assess the general variability of each biomarker throughout the record (Fig. 6). Relative distributional changes were additionally compared to modern assemblages observed in Barents Sea surface sediments characterised by contrasting overlying SpSIC and annual open water duration (Fig. 7; Belt et al., 2015; Köseoğlu et al., 2018a). The SpSIC database represented April–June SIC spanning the 1988–2007 period, previously used to build the CT model (Köseoğlu et al., 2018a).

5. Results

5.1. Biomarker temporal profiles and distributions in core GS14

Following an initial increase from ca. 25.8 cal kyr BP, IP_{25} and HBI II concentrations reached their respective peak values of 7.5 and 43.7 ng g^{-1} by ca. 23.7 cal kyr BP (Fig. 3a). This coincided with a similar increase of all six sterols during the same period, which culminated between 24.7 and 23.7 cal kyr BP. Both sympagic HBIs (i.e. IP_{25} and HBI II) and all sterols remained at relatively high, but variable concentrations until 18.0 cal kyr BP (Figs. 3, 4 and 6b), while concentrations of HBI trienes III and IV remained low (0.7 ± 0.5 ng g^{-1} and 0.6 ± 0.5 ng g^{-1}, respectively; Fig. 6a). Accordingly, the HBI assemblage was dominated by IP_{25} and HBI II, with respective percentage contributions of $13 \pm 2\%$ and $80 \pm 5\%$, while HBIs III and IV were only minor constituents throughout the 25.8–18.0 cal kyr BP interval (Fig. 7a). This was accompanied by average $P_{III}IP_{25}$ SpSIC estimates of $74 \pm 9\%$ and consistently

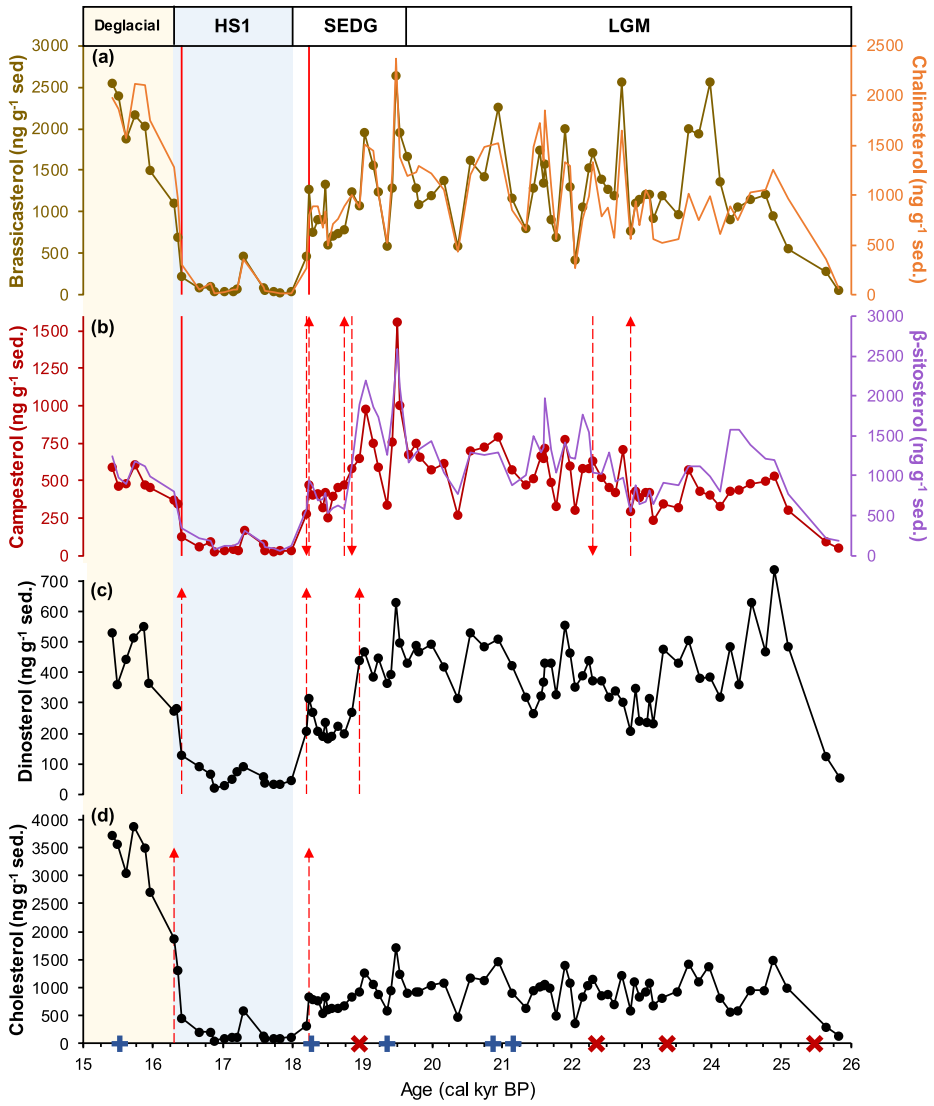


Fig. 4. Sterol concentration profiles for core GS14: (a) Brassicasterol and chalinasterol; (b) Campesterol and β-sitosterol; (c) Dinosterol; (d) Cholesterol. In all plots, coloured background bands constrain the LGM and SEDG (25.8–18.0 cal kyr BP), HS1 (18.0–16.3 cal kyr BP) and Deglacial (after 16.3 cal kyr BP) time slices. Changepoints significant at a 99.5% confidence level ($p < 0.005$) are shown by vertical red lines, where upward or downward pointing dashed arrows apply to the left and right y-axis, respectively, while a solid line applies to both left and right y-axes. Red and blue crosses highlight GS14 and GC08 ^{14}C AMS dates on the age scale, respectively. (For interpretation of the references to colour in this figure legend, the reader is referred to the Web version of this article.)

extensive sea ice conditions predicted by the CT model (Fig. 3c). However, SpSIC values < 60% with sporadic summer sea ice occurrence ca. 19.2–18.7 cal kyr BP and CT predictions of intermediate (MIZ-like) sea ice conditions accompanied slight, but abrupt decreases in sympagic HBI and sterol concentrations, with the more distinct changes also highlighted by changepoint analysis (Figs. 3a and 4). Finally, examination of the sterol distribution revealed the prevalence of β-sitosterol (23 ± 6%) and epibrassicasterol (23 ± 5%), with moderate cholesterol (18 ± 3%) and chalinasterol (19 ± 4%), as well as relatively minor campesterol (10 ± 2%) and dinosterol (7 ± 2%) until 18.0 cal kyr BP (Fig. 7b).

Precipitous and abrupt decreases of all biomarker concentrations characterised the 18.0–16.3 cal kyr BP interval and were detected by changepoint analysis (Figs. 3 and 4). Thus, averaged HBI and sterol concentrations ranged from 0.2 to 2.2 ng g^{-1} and 57–182 ng g^{-1}, respectively (Fig. 6) despite brief increases in IP_{25} and HBI II to ca. 2.9 ng g^{-1} and 10.9 ng g^{-1}, respectively (Fig. 3a). The interval was also characterised by the highest SpSIC estimates (ca. 90%), summer sea ice occurrence, and CT predictions of extensive sea ice conditions (Fig. 3c). Biomarker percentage distributions remained similar to those observed during the 25.8–18.0 cal kyr BP interval, albeit with more variability and, in case of sterols, prevalence of β-sitosterol alongside cholesterol (Fig. 7).

An abrupt increase of biomarker concentrations, with significant shifts in percentage distributions and sea ice conditions are evident after ca. 16.3 cal kyr BP. $P_{III}IP_{25}$-derived SpSIC values dropped to a minimum of 4 ± 11%, and the CT model consistently predicted marginal ice cover or open water conditions (Fig. 3c). HBIs III and IV increased by ca. 2 orders of magnitude to the highest values observed throughout the record (29.1 ± 24.4 ng g^{-1} and 48.2 ± 41.8 ng g^{-1}, respectively), while IP_{25} and HBI II remained at respective minimum values of 0.6 ± 0.3 ng g^{-1} and 3.2 ± 1.5 ng g^{-1} (Fig. 6a). Consequently, HBIs III and IV dominated the HBI distribution during this period, with relative abundances of 33 ± 8% and 53 ± 14%, respectively (Fig. 7a). The sterols experienced a similar, but less pronounced resurgence, with most exhibiting

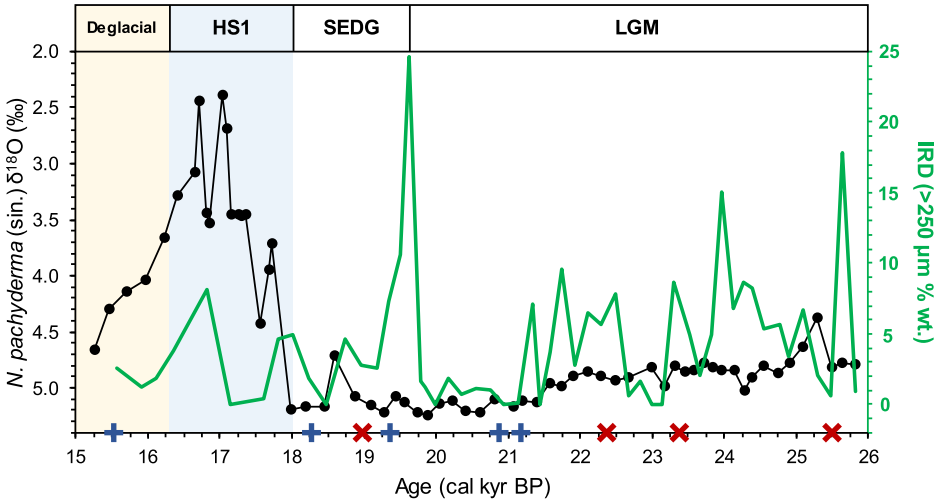


Fig. 5. Planktic $\delta^{18}O$ of *N. pachyderma* sin. (black line with circle markers) and IRD data (green line) for core GS14, obtained from Knies et al. (2018). Red and blue crosses highlight GS14 and GC08 ^{14}C AMS dates on the age scale, respectively. (For interpretation of the references to colour in this figure legend, the reader is referred to the Web version of this article.)

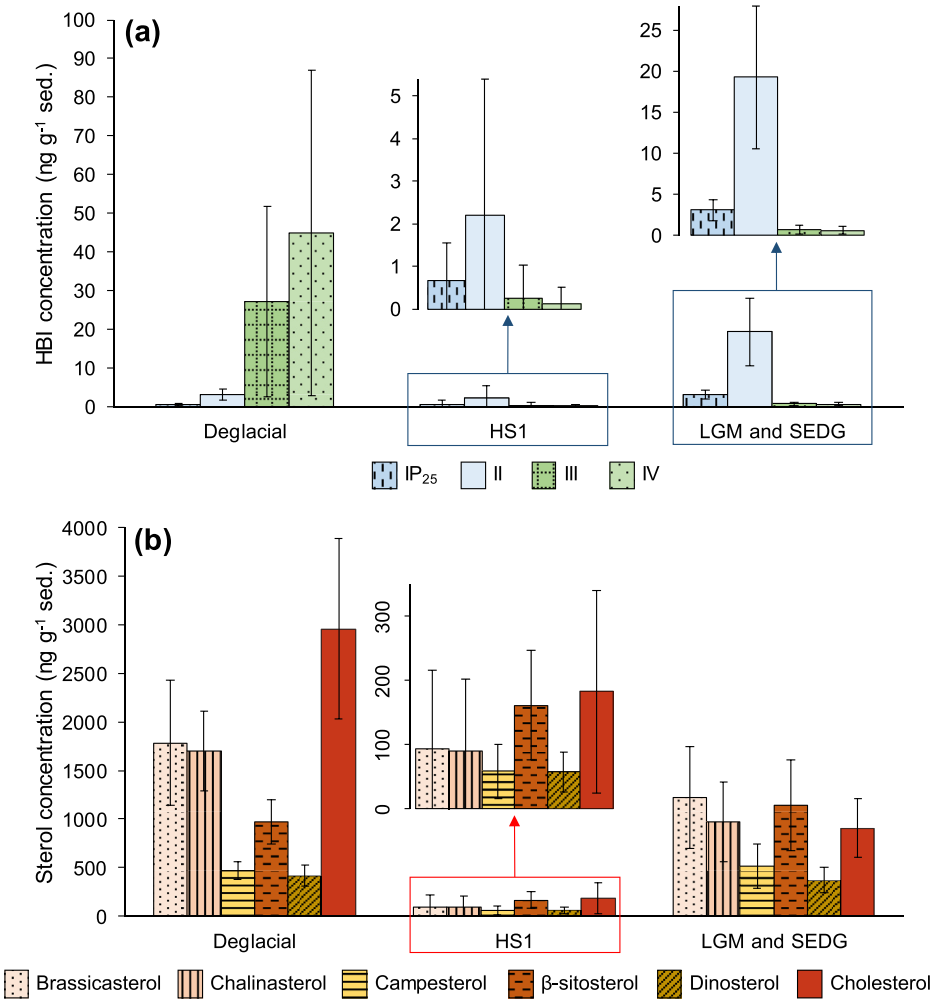


Fig. 6. Concentration distributions during the LGM (with SEDG), HS1, and Deglacial for: (a) HBIs; (b) Sterols. Error bars denote ±1 sample SD in each case. Blue and red boxes with outgoing arrows show plot areas zoomed in for clarity for HBIs and sterols, respectively. (For interpretation of the references to colour in this figure legend, the reader is referred to the Web version of this article.)

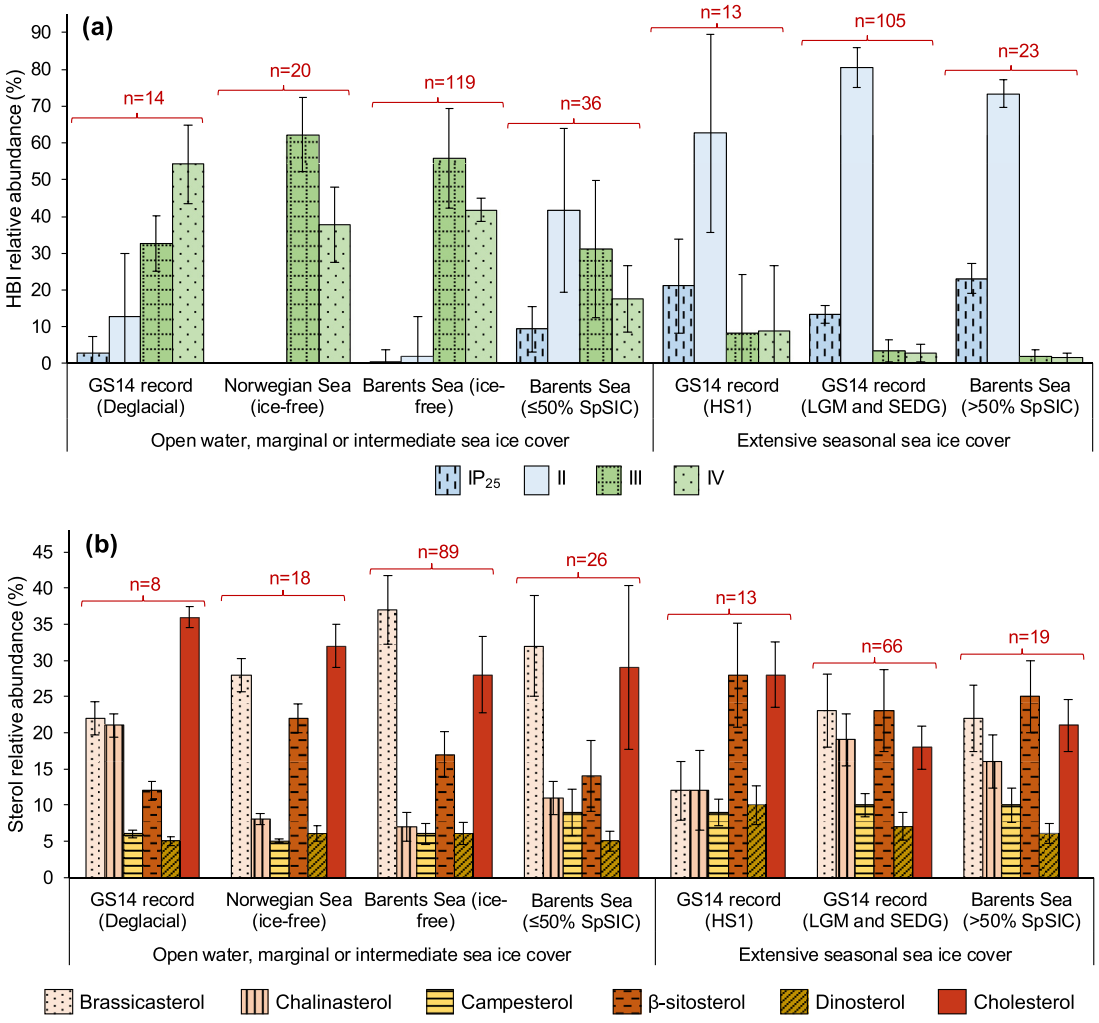


Fig. 7. Relative abundance distributions during the LGM (with SEDG), HS1, and Deglacial for: (a) HBIs, with comparisons to modern distributions reported in Barents and Norwegian Sea surface sediments characterised by contrasting sea ice regimes (Fig. 1b); (b) Sterols, with comparisons to surface sedimentary distributions analogous to those in (a). Error bars denote ±1 sample SD for each biomarker, while the sample size n is shown in red above each distribution. (For interpretation of the references to colour in this figure legend, the reader is referred to the Web version of this article.)

concentrations similar to those observed prior to 18.0 cal kyr BP (Figs. 4 and 6c). The greatest concentration increase was observed for cholesterol, which reached a mean value of ca. 2957 ± 930 ng g^{-1} (Figs. 4d and 6b), a factor ca. three higher than the 25.8–18.0 cal kyr BP average (904 ± 302 ng g^{-1}). Cholesterol therefore dominated the sterol assemblage with $36 \pm 1\%$ relative abundance instead of epibrassicasterol and β-sitosterol, which contributed $22 \pm 2\%$ and $12 \pm 1\%$, respectively. Consistently with the remainder of the record, chalinasterol abundance ($21 \pm 2\%$) was comparable to that of epibrassicasterol, while campesterol ($6 \pm 1\%$) and dinosterol ($5 \pm 1\%$) remained minor components (Fig. 7b).

5.2. Surface sediment biomarker distributions

HBI distributions in surface sediments (Fig. 7a) characterised by extensive sea ice cover (>50% SpSIC; $n = 23$) were characterised by a distinct prevalence of IP_{25} and HBI II within the assemblage ($23 \pm 4\%$ and $73 \pm 4\%$, respectively), with minor contribution from HBIs III and IV ($2 \pm 2\%$ and $2 \pm 1\%$, respectively). The contribution of sympagic biomarkers was lower and more variable in the central Barents Sea MIZ (≤50% SpSIC; $n = 36$), with respective percentage abundances of $9 \pm 6\%$ and $42 \pm 22\%$ observed for IP_{25} and HBI II. Accordingly, pelagic HBIs III and IV comprised a higher $31 \pm 19\%$ and $18 \pm 9\%$ of the assemblage, respectively. Ice-free Barents ($n = 119$) and Norwegian Sea ($n = 20$) locations were characterised almost entirely by HBIs III ($56 \pm 14\%$ and $62 \pm 10\%$, respectively) and IV ($42 \pm 3\%$ and $38 \pm 10\%$, respectively), while only 4 locations close to the annual maximum sea ice edge in the Barents Sea exhibited non-zero IP_{25} and HBI II.

Sterol distributions were mainly defined by the variability of β-sitosterol, epibrassicasterol, and cholesterol in all surface sediments. Conversely, chalinasterol, campesterol, and dinosterol remained minor components (Fig. 7b). Extensively ice-covered locations showed a prevalence of β-sitosterol ($25 \pm 5\%$), with comparable, but slightly lower abundances of cholesterol ($21 \pm 4\%$) and epibrassicasterol ($22 \pm 5\%$). Conversely, MIZ and ice-free Barents Sea locations ($n = 26$ and $n = 89$, respectively) exhibited decreased β-sitosterol abundance (14–17 ± 3–5%), with epibrassicasterol (32–37 ± 5–7%) and cholesterol (28–29 ± 5–11%) comprising most of the assemblage. Norwegian Sea sediments ($n = 18$) showed consistent prevalence of cholesterol ($32 \pm 3\%$), with similar epibrassicasterol content ($28 \pm 2\%$) and lower β-sitosterol ($22 \pm 2\%$).

6. Discussion

Biomarker data presented herein allow us to reconstruct seasonal sea ice and productivity variability during climatically contrasting conditions encompassing both growth and decay of the BSIS. To facilitate paleo-interpretation and contextualisation, we delineate the GS14 record into discrete time slices, and include a rationale for these in section 6.1. Paleo-interpretation for each time slice is then provided in section 6.2–6.4.

6.1. Identification of time slices for core GS14

Our record is delineated into three main time slices: (i) The LGM and initial shelf edge deglaciation (SEDG) following ice sheet destabilisation (ca. 26.0–18.0 cal kyr BP); (ii) HS1 following final BSIS collapse (ca. 18.0–16.3 cal kyr BP); (iii) The retreat of sea ice cover (ca. 16.3 cal kyr BP) preceding AMOC recovery and the onset of the Bølling-Allerød (BA) interstadial. The time slice definitions are based on a combination of clear changes of biomarker concentrations (Figs. 3 and 4) and percentage distributions (Figs. 6 and 7), and the agreement between the timing of these changes in core GS14 and paleoceanographic shifts previously identified in the Barents Sea and other Arctic regions. The definitions of the LGM, SEDG, and the HS1 onset are based on the study of Knies et al. (2018), who infer a BSIS advance to its LGM shelf-edge position at ca. 26.0 cal kyr BP from increased sedimentation rates and IRD deposition. This also agrees with previous global definitions of Peltier and Fairbanks (2006) and Clark et al. (2009), who propose LGM onset at 26 cal kyr BP and 26.5 cal kyr BP, respectively. An IRD spike marks the SEDG at ca. 19.5 cal kyr BP, while final BSIS collapse between ca. 18.0–17.7 cal kyr BP is associated with a rapid, meltwater-induced planktic $\delta^{18}O$ depletion signifying the beginning of HS1 (Fig. 5) (Knies et al., 2018) and is also observed in various records from the Barents Sea, the Nordic Seas (Elverhøi et al., 1995; Dokken and Jansen, 1999; Bauch et al., 2001; Weinelt et al., 2003; Müller and Stein, 2014), and other Arctic seas (e.g. Jennings et al., 2018). In our study, we additionally note the abrupt decreases of all biomarker concentrations by 18.0 cal kyr BP (Figs. 3 and 4), and use this date as the beginning of the HS1. Finally, the post-HS1 deglacial period is defined by significant and contemporaneous changes in biomarker concentrations (Fig. 3b and c and 4) and relative abundances (Figs. 6 and 7) in core GS14 at ca. 16.3 cal kyr BP.

6.2. BSIS-adjacent productive ice margin during the LGM and SEDG (26–18 cal kyr BP)

Based on high dinosterol and IP_{25} concentrations, Knies et al. (2018) previously provided direct evidence of highly-productive coastal polynyas at the GS14 site during the otherwise harsh glacial conditions of the LGM. Such polynyas initiated by AW upwelling and maintained by powerful katabatic winds from the BSIS were previously suggested to significantly influence Late Weichselian sea ice and primary productivity regimes across the western (Müller et al., 2009; Müller and Stein, 2014; Xiao et al., 2015) and northern Barents Sea margins (Chauhan et al., 2016; Knies et al., 1999, 2018; Nørgaard-Pedersen et al., 2003). Our findings of abundant sympagic biomarkers (IP_{25} and II; Fig. 3a) with presence of pelagic HBIs III and IV (Fig. 3b) and high sterol concentrations (Fig. 4) support the existence of extensive, but seasonal sea ice (Fig. 3c), high overall productivity, and vertical stabilisation necessary to maintain pelagic spring and summer blooms at the GS14 site (e.g. Falk-Petersen et al., 2000; Signorini and McClain, 2009; Wassmann et al., 1999). This is further corroborated by the similarity of both the overall HBI and sterol assemblages in our record during the LGM and SEDG to that of northern and north-eastern Svalbard (Fig. 7) – an ice-covered region characterised by seasonally open waters during the summer (Fetterer et al., 2017; Köseoğlu et al., 2018a, 2018b; Vare et al., 2010), as well as WSC-mediated winter polynya (Ivanov et al., 2012) and a high overall lead fraction (Willmes and Heinemann, 2016) facilitating light penetration and development of under-ice pelagic blooms (Assmy et al., 2017; Strass and Nöthig, 1996). Moreover, average LGM and SEDG concentrations of pelagic HBIs III and IV (0.7 ng g^{-1} and 0.6 ng g^{-1}, respectively) and sterols (0.37–1.22 μg g^{-1}) in our record (Fig. 6) are also similar to those we observe in surface sediments north and north-east off Svalbard (0.5–0.6 ng g^{-1} and 0.63–2.67 μg g^{-1} for HBIs and sterols, respectively). Thus, we confirm the incidence of coastal polynya at the GS14 site throughout 26–18 cal kyr BP, which is also potentially associated with previously inferred sub-surface AW inflow in the Nordic Seas throughout ca. 27–22.5 cal kyr BP, at least (Chauhan et al., 2016; Dokken and Hald, 1996; Hebbeln et al., 1994; Knies et al., 1999; Nørgaard-Pedersen et al., 2003; Rasmussen et al., 2007; Rørvik et al., 2013; Vogt et al., 2001). Additionally, several investigations report high primary productivity with seasonally open waters evident from coevally high pelagic and sympagic biomarker concentrations along western Svalbard, Yermak Plateau (e.g. Kremer et al., 2018a, 2018b; Müller et al., 2009; Müller and Stein, 2014; Rasmussen et al., 2007) and other Arctic regions (Stein et al., 2017), presence of temperate benthic foraminifera west and north off Svalbard (Chauhan et al., 2016), and decreasing planktonic foraminiferal and IRD abundances from the Fram Strait towards the Central Arctic Ocean (Nørgaard-Pedersen et al., 2003).

The insolation-induced BSIS destabilisation at the GS14 site began at ca. 19.5 cal kyr BP (Knies et al., 2018), as indicated by increased IRD input; surface meltwater influence was likely absent or limited at this time, as no planktic $\delta^{18}O$ depletions were observed (Fig. 5). High IRD input could have diluted biogenic sedimentation, resulting in the slightly decreased sympagic (e.g. IP_{25}) and pelagic (sterols) primary productivity at the core site (Fig. 3a and b, 4). Nonetheless, seasonal sea ice conditions that characterised the earlier LGM (26.0–19.7 cal kyr BP) persisted, with frequent summer sea ice occurrence (Fig. 3c).

6.3. Productivity termination during Heinrich Stadial HS1 (18.0–16.3 cal kyr BP)

Precipitous decreases of all biomarker concentrations to minimum values observed throughout the record (Figs. 3 and 4) and maximum $P_{III}IP_{25}$-derived SpSIC with extensive sea ice conditions predicted by the CT model (Fig. 3c) support the presence of closed perennial sea ice cover with near-zero primary productivity at the core site between ca. 18–16.3 cal kyr BP (Knies et al., 2018). While a brief increase in sympagic HBIs to late LGM levels at 17.2 cal kyr BP potentially indicates sufficient thinning of sea ice cover to initiate photosynthesis during the summer (Fig. 3a), the overall onset of harsh conditions agrees with the widespread collapse of NH ice sheets at ca. 17.5 cal kyr BP following continued increases of summer insolation and sea level (Yokoyama et al., 2000; Clark et al., 2009; Shakun et al., 2012), strong ice stream activity (Winsborrow et al., 2010) and AW-induced weathering of the BSIS grounding line (Hormes et al., 2013). Contemporaneous massive meltwater discharges from icebergs are evidenced between ca. 17.7–16.9 cal kyr BP by depleted planktic $\delta^{18}O$ and dominance of *N. pachyderma* (sin.) across the Norwegian Sea (Hoff et al., 2016; Rasmussen and Thomsen, 2008; Thornalley et al., 2015), south-western Barents Sea (Rasmussen et al., 2007) and Svalbard (Chauhan et al., 2016; Jessen et al., 2010; Koç et al., 2002). Accordingly, decreased planktic $\delta^{18}O$ values observed in the GS14

record after ca. 18.0 cal kyr BP (Fig. 5) were previously attributed to meltwater-induced cooling and freshening of surface waters due to BSIS collapse (Knies et al., 2018), promoting stratification and sea ice re-expansion in the Barents Sea. Meltwater influence hampered the AMOC (McManus et al., 2004; Ritz et al., 2013), causing a reduction in NAC-bound AW inflow evident from depleted benthic $\delta^{18}O$ values across the Nordic Seas (Bauch et al., 2001; Knies et al., 2001; Rasmussen and Thomsen, 2008). Thus, our findings support the conclusions of Knies et al. (2018) that the combined influence of cold, low-salinity surface waters, a strongly stratified water column, and a hindered AW inflow into the Barents Sea following BSIS disintegration facilitated perennial sea ice formation and limited the volume and upwelling of deep nutrient-rich waters to the photic zone (Fig. 8b). We argue that insufficient nutrient replenishment combined with reduced light penetration through thick multi-year ice following the closing of coastal polynya potentially caused a collapse of microalgal stocks – a scenario previously shown by modelling simulations (Schmittner, 2005) that likely resulted in near-zero biomarker concentrations in our dataset from ca. 18.0–16.3 cal kyr BP (Figs. 3, 4 and 6). Indeed, similarly to the LGM, the relative distributions of HBIs (Fig. 7a) remain consistent with modern assemblages indicative of extensive sea ice conditions North-East off Svalbard (Köseoğlu et al., 2018a), which suggests that primary productivity was still controlled by sea ice. The sterol distribution, however, slightly deviates from that of the north-eastern Svalbard surface sediments (Fig. 7b) due to dominance of cholesterol alongside β-sitosterol. The inhospitable conditions of thick ice cover during the HS1 likely reduced algal biodiversity – a trend observed at higher Arctic latitudes today (Falk-Petersen et al., 1998; Henderson et al., 1998). Thus, the change in sterol distribution probably reflects a shift in the algal assemblage, especially given their ubiquity (Belt et al., 2013; Belt, 2018; Volkman, 2003). For instance, spring blooms in the Central Arctic Ocean are often dominated by the cold-adapted diatom *M. arctica* (Syvertsen, 1991; Boetius et al., 2013), while at least some *Melosirales* produce both β-sitosterol and cholesterol as the two major sterols (Rampen et al., 2010). In any case, the presence of perennial ice overlying the study area is further substantiated by the absence of significant IRD input (Fig. 5) and low sedimentation rates of ca. 12 cm kyr^{-1} throughout the 18.0–16.3 cal kyr BP interval in core GS14 (Knies et al., 2018).

6.4. Ice retreat and intense productivity after 16.3 cal kyr BP

Considerable increases in absolute concentrations of pelagic HBIs (Figs. 3b and 6a) and sterols (Figs. 4 and 6b), accompanied by shifts in respective percentage distributions (Fig. 7) indicated a general climate amelioration with enhanced primary productivity and SpSIC <10% (Fig. 3c) after 16.3 cal kyr BP. Low concentrations of sympagic IP_{25} and HBI II therefore shift the relative distribution to favour HBIs III and IV, which agrees with the modern HBI assemblage representing nearly ice-free settings with prolonged open water duration (Fig. 7a). Together with decreased $P_{III}IP_{25}$-derived SpSIC with CT predictions of marginal sea ice conditions (Fig. 3c; Köseoğlu et al., 2018a; Smik et al., 2016) and an abrupt increase of IRD at ca. 16.3 cal kyr BP (Knies et al., 2018), our evidence suggests limited annual sea ice cover (<10% SpSIC) and sympagic productivity (e.g. Belt et al., 2007; Belt and Müller, 2013; Brown et al., 2014b), with favourable conditions for pelagic blooms and the GS14 site being close to the annual maximum ice edge (Belt et al., 2015, 2017). Rapid sea ice and areal BSIS retreat is also apparent throughout the Barents Sea continental shelves between ca. 16.5–15.5 cal kyr BP, inferred from the abundance of opportunistic benthic foraminifera characteristic of productive waters (Chauhan et al., 2016), increased IRD deposition and meltwater release from sea ice and icebergs (e.g. Chauhan et al., 2016; Jessen et al., 2010; Knies and Stein, 1998; Vogt et al., 2001), as well as high biomarker concentrations (e.g. Müller and Stein, 2014) around Svalbard. Since ca. 17.5 cal kyr BP, a gradual increase in insolation (Berger and Loutre, 1991; Laskar et al., 2004) probably contributed to the areal retreat of the BSIS and reinvigoration of the AMOC at ca. 16 cal kyr BP (McManus et al., 2004; Ritz et al., 2013) following a reduction of glacial meltwater flux also evident from modelling studies (e.g. Liu et al., 2009). The deglaciation was potentially also triggered by progressive aridification of the Arctic during HS1 due to limited ocean-atmosphere heat and moisture exchange through perennial ice cover (e.g. Hormes et al., 2013), which reduced the moisture supply for ice sheet build-up. Ice streams retreated from the western Barents Sea margin due to a shifting BSIS mass balance after ca. 17 cal kyr BP (Winsborrow et al., 2010), which contributed to a separation of the BSIS and FIS in the central Barents Sea (Newton and Huuse, 2017). Thus, we suggest that precipitous sea ice retreat from the western Barents Sea continental slope at ca. 16.3 cal kyr BP coincided with the eastbound areal deglaciation of the BSIS (Fig. 8c).

Conspicuous enhancement of pelagic HBI concentrations (Figs. 3b and 6a) towards values > 140 ng g^{-1} is unprecedented both within the GS14 record and the contemporary Barents Sea, where maximum sedimentary concentrations of HBIs III and IV detected in the highly-productive MIZ do not exceed ca. 47 and 22 ng g^{-1}, respectively (Belt et al., 2015; Köseoğlu et al., 2018a). Such a remarkable increase in pelagic diatom productivity at the GS14 site after ca. 16.3 cal kyr is in broad agreement with Wollenburg et al. (2004), who also found that paleoproductivity in relatively fresh surface waters surpassed modern averages at the northern Svalbard margin during this period. Additionally, benthic foraminiferal assemblages along the continental margin adapted to warm AW and increased nutrient availability (e.g. Chauhan et al., 2016). Together, these data suggest the existence of significantly more productive post-HS1 conditions compared to those spanning at least the last several decades of sedimentation in the MIZ (Belt et al., 2015; Köseoğlu et al., 2018a), and are unlikely to be solely attributable to sea ice retreat and establishment of a productive seasonal ice margin following HS1.

Several factors could have renewed pelagic productivity. The stratified water column in the Arctic throughout HS1 was initially salinity-controlled due to deglacial meltwater input since ca. 20–19 cal kyr BP (e.g. Chauhan et al., 2016; Hoff et al., 2016; Jennings et al., 2018; Jessen et al., 2010; Rasmussen et al., 2007; Rasmussen and Thomsen, 2008), which hampered the AMOC and NADW formation (Gherardi et al., 2009; McManus et al., 2004), slowing deep water ventilation in the North Atlantic and the Nordic Seas (Thiagarajan et al., 2014; Thornalley et al., 2015). Thus, a combination of reduced convective heat loss from northbound bottom waters due to strong salinity-driven stratification, and geothermal heating (e.g. Adkins et al., 2005) potentially caused a basin-wide increase of subsurface water temperatures according to proxy-based (Cronin et al., 2012; Thiagarajan et al., 2014) and modelling studies (Liu et al., 2009). Indeed, millennial sub-surface warming of 2–3 °C since ca. 19 cal kyr BP is supported by foraminiferal transfer function reconstructions (Rørvik et al., 2013), Δ_{47} clumped isotope data, increased Mg/Ca ratios (Cronin et al., 2012; Thiagarajan et al., 2014; Thornalley et al., 2015), and benthic $\delta^{18}O$ depletions (e.g. Rasmussen and Thomsen, 2004) across the Nordic Seas. Similar warming along the Barents Sea and Svalbard margins is indicated by intrusion of temperate benthic foraminifera adapted to reduced productivity immediately prior to the HS1 (Chauhan et al., 2016; Rasmussen et al., 2007; Wollenburg et al., 2004), which potentially affected the GS14 site and contributed to BSIS debuttressing, triggering glacial conditions at the onset of HS1 (e.g.

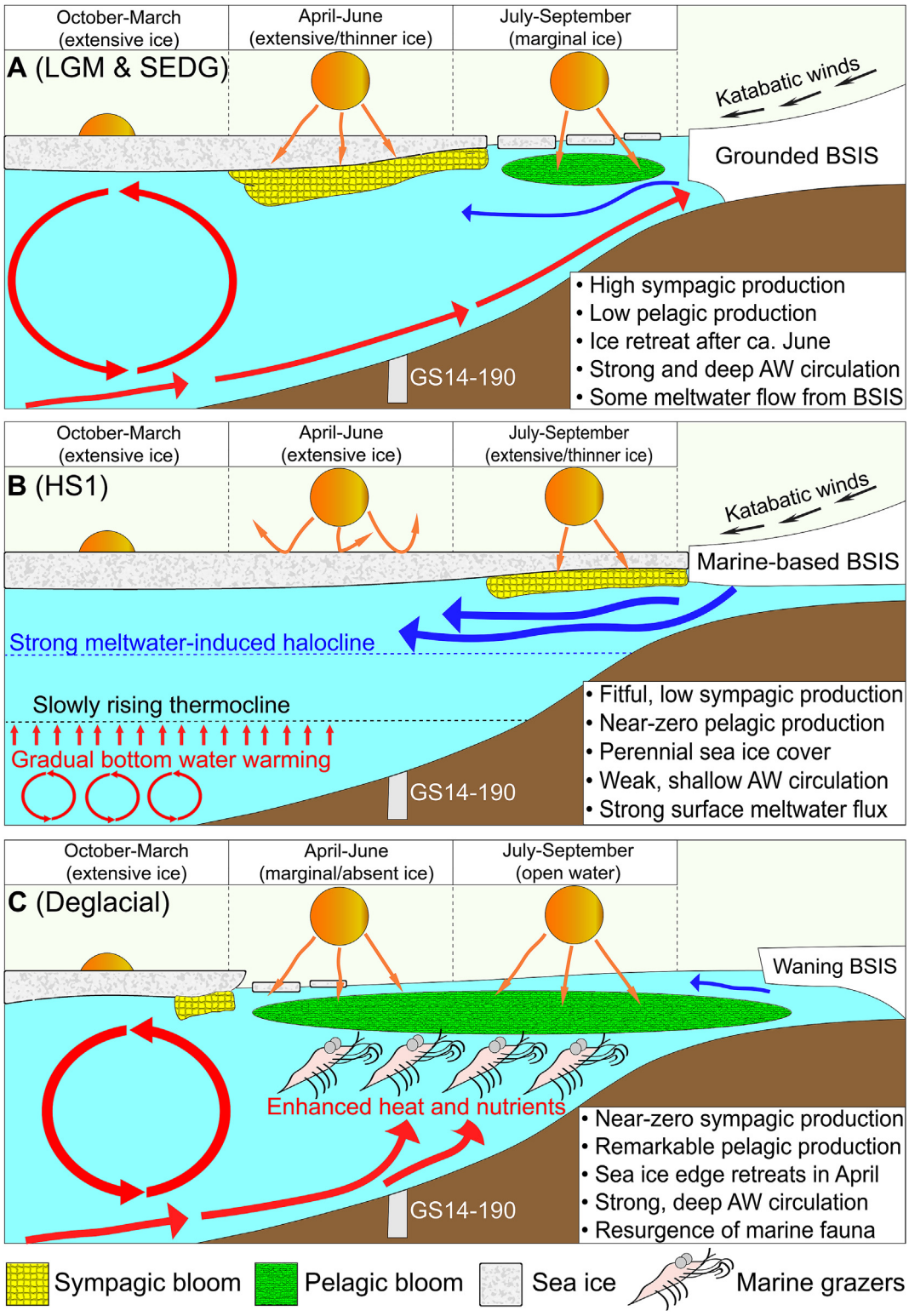


Fig. 8. Conceptual representation of sea ice and productivity conditions at the southwestern Barents Sea continental slope throughout: (A) The LGM and SEDG (25.8–18.0 cal kyr BP); (B) The HS1 (18.0–16.3 cal kyr BP); (C) The Deglacial (16.3 cal kyr BP onwards). Seasonal sea ice conditions inferred from SpSIC (%) and the CT model are illustrated during winter (October–March), spring (April–June) and summer (July–September). Red and blue arrows correspond to AW and meltwater fluxes, respectively, where line width increases with flow strength. Orange arrows represent solar insolation. (For interpretation of the references to colour in this figure legend, the reader is referred to the Web version of this article.)

Hormes et al., 2013; Marcott et al., 2011). Such accumulation of subsurface heat in a salinity-stratified water column lowers the density of deep waters – a thermobaric effect which positively scales with pressure – and gradually destabilises the column by reducing the depth threshold at which the cold surface waters become denser than the warm, saline waters below. Once the depth threshold is breached, overturning resumes as the cold surface waters accelerate downwards, while the heat and salt accumulated in the deep waters is rapidly released to the surface ocean (e.g. Adkins et al., 2005). Such phenomena have been recorded in the Norwegian Sea, where subsurface temperatures rapidly decreased between ca. 18–15 cal kyr BP following a period of millennial warming (Rørvik et al., 2013; Thornalley et al., 2015). We therefore suggest that intense, instability- or buoyancy-driven upwelling of warm and saline subsurface waters at the GS14 site could have made massive surface reservoirs of heat and nutrients available (Fig. 8c) for seasonal ice melting (Fig. 3c) and unprecedented pelagic productivity (Fig. 3b) after 16.3 cal kyr BP. Increased nutrient availability and efficient surface enrichment activated by this overturning resumption was potentially maintained by the deepening and intensification of the AMOC towards the Bølling-Allerød warming at ca. 15 cal kyr BP (McManus et al., 2004; Ritz et al., 2013; Shakun et al., 2012). Additionally, in contrast to the slow development of stratification and pelagic productivity in the ice-free southwestern Barents Sea today due to strong NAC- and wind-driven vertical mixing (Wassmann et al., 1999), the post-HS1 productive season at the GS14 site could have been prolonged and hastened by earlier stratification due to meltwater input from sea ice and BSIS retreat (Hormes et al., 2013). Influx of ice and iceberg-entrained terrigenous material from coastal erosion could have provided an additional nutrient supply, as previously noted for the postglacial western (Aagaard-Sørensen et al., 2010) and northern Barents Sea (Knies and Stein, 1998). Thus, a combination of marginal seasonal sea ice, surface warming, hastened meltwater-fuelled stratification, and an augmented nutrient input from terrigenous material and intense upwelling potentially stabilised pelagic species longer in the photic zone and reduced nutritional limitation during the peak bloom, explaining the GS14 productivity trends (Fig. 8c). Although it is not feasible to decouple the relative influences of individual factors, the core site was probably characterised by a significantly different productivity regime relative to the ephemeral, nutrient-limited blooms that occur in the modern Barents Sea (Signorini and McClain, 2009), where the phytoplankton productivity increase of recent years is mainly driven by a strengthening AW inflow (Årthun et al., 2012) and reducing sea ice extent (Arrigo and van Dijken, 2015; Assmy et al., 2017), and is not influenced by increased meltwater and terrigenous matter fluxes.

High sterol concentrations after ca. 16 cal kyr BP resemble the trend of abruptly increasing pelagic HBI concentrations (Figs. 3b and 4) and support our assumption of renewed primary productivity at the core site following precipitous ice retreat (Figs. 3c and 8c). While most sterols only reach pre-HS1 values at the core site, cholesterol concentrations increase by a factor of 3 relative to LGM values and dominate the percentage distribution at 36% relative abundance instead of β-sitosterol (Figs. 6b and 7b). Similarly to HS1, this could simply be attributable to a switch in the algal assemblage to favour cholesterol production (e.g. by centric diatoms; Rampen et al., 2010). Another explanation is the efficient conversion of algal sterols to cholesterol by auxotrophic consumers, including zooplankton, which potentially flourished after the HS1 due to resumed deep circulation (Gherardi et al., 2009; McManus et al., 2004; Ritz et al., 2013) and global atmospheric-oceanic warming (Shakun et al., 2012). Zooplankton at lower trophic levels extensively feed on pelagic and sympagic algae for growth and reproduction, with increased grazing rates characteristic of warm and highly-productive conditions with large phytoplankton stocks (Falk-Petersen et al., 2000; Tamelander et al., 2008). Contemporary zooplankton communities in the Barents Sea MIZ during peak blooms are dominated by crustaceans, including copepods and krill (e.g. Eriksen et al., 2017), which require a continuous source of cholesterol to maintain their phospholipid membranes and produce offspring (Hassett and Crockett, 2009). Accordingly, cholesterol is invariably the major constituent (usually >50%) of sterol distributions in Arctic and Antarctic crustaceans (Hamm et al., 2001; Mühlebach et al., 1999). Herbivorous and omnivorous arthropods largely rely on chemical conversion of phytosterols to cholesterol, which they cannot biosynthesize (Goad, 1981; Martin-Creuzburg and von Elert, 2009) or obtain in sufficient quantity from an algal diet. Therefore, it is possible that the nutrient-replete and diatom-rich conditions inferred from high pelagic HBI (III and IV) concentrations at the GS14 site after HS1 (Fig. 3b) revitalised zooplankton production and phytosterol to cholesterol bioconversion, leading to the proportionally larger increases of the latter sterol (Fig. 4). Additionally, our suggestion of a warming water column due to intensive post-HS1 circulation of sub-surface heat could have accelerated zooplankton metabolism, switching from temperature-limited to nutrient-limited growth with increased nutritional and reproductive cholesterol requirements (Hassett and Crockett, 2009). Overall, increased phytosterol conversion rates and zooplankton stocks following the post-HS1 climate amelioration represent one plausible mechanism for the switch from a phytosterol-to cholesterol-defined sterol assemblage after 16 cal kyr BP. Notably, however, such a cholesterol-dominated sterol distribution is not reproduced in the contemporary Barents Sea, where epibrassicasterol abundances increase alongside those of cholesterol, and are often higher. Consistent cholesterol prevalence is only observed in the warmer Norwegian Sea (Fig. 7b) characterised by significant transport of copepods and krill with the NAC (Falk-Petersen et al., 2000), contributing to their role as major pelagic food web components in the Barents Sea (Aarflot et al., 2017; Eriksen et al., 2017). These observations potentially indicate that the highly-productive post-HS1 interval in the GS14 record is unique and not reproduced in the contemporary Barents Sea, supporting similar suggestions based on the unprecedented increase of pelagic HBIs III and IV, which overshadows that of cholesterol (Figs. 3b, 4d and 7).

7. Conclusions

Geochemical biomarkers in a marine sediment core provided new insights into the abruptly shifting seasonal sea ice conditions and primary productivity regimes on the southwestern Barents Sea slope throughout ca. 26–15 cal kyr BP. We draw the following main outcomes:

1) The LGM interval and initial SEDG were characterised by extensive sea ice covering the site, with seasonal occurrence of highly-productive coastal polynya. Overall marine productivity was variable, but generally high until 18.0 cal kyr BP.
2) The onset of perennial sea ice cover during HS1 coincides with widespread NH ice sheet collapse and large meltwater influx at ca. 18.0 cal kyr BP as a result of AW-induced basal melting, atmospheric aridification and increased iceberg calving due to sea level rise. Thus, overall productivity plummeted until ca. 16.3 cal kyr BP as a result of a pan-Arctic meltwater-induced pycnocline, abrupt AMOC weakening and reduced light penetration through newly-formed perennial sea ice.
3) Coincident with a rapid sea ice retreat to values < 10% SpSIC between ca. 16.3–16.1 cal kyr BP, primary productivity exceeded the most productive contemporary conditions in the Barents Sea

MIZ. This feature is likely uniquely deglacial and attributable to heat and nutrients released to the surface waters due to thermobaric and/or buoyancy-triggered instabilities following subsurface warming under weak thermohaline circulation of the HS1. Meltwater input and coastal erosion from the BSIS could have provided an additional nutrient supply to the pelagic environment. We tentatively infer a revitalisation of marine fauna due to vast increases of algal biomass and surface warming.

4) We note some consistency of relative biomarker distributions downcore with those observed in contrasting sea ice and primary productivity regimes of the contemporary Barents Sea. We are able to decouple sympagic and pelagic primary production using source-specific HBI biomarkers characteristic of ice algal and pelagic diatoms, which indicate that LGM productivity was predominantly ice-based, while post-HS1 production conversely relied on free-floating pelagic algae with minor contribution from sympagic sources. In contrast, sterol concentrations remained similar under seasonal sea ice conditions of the LGM and the post-HS1 deglaciation, and likely represent a mixed algal source.

Data availability

Datasets related to this article can be found at doi: https://doi.org/10.17632/jx97c9nv3k.1, hosted at Mendeley Data.

Acknowledgements

We are grateful to Marta Rodrigo-Gámiz and two anonymous reviewers for their comments, which greatly helped improve the focus and presentation of the manuscript. This research was jointly supported by the Research Council of Norway (Centre of Excellence scheme for CAGE; project 223259) and the University of Plymouth.

Appendix A. Supplementary data

Supplementary data to this article can be found online at https://doi.org/10.1016/j.quascirev.2019.105903.

References

Aagaard-Sørensen, S., Husum, K., Hald, M., Knies, J., 2010. Paleoceanographic development in the SW Barents Sea during the late Weichselian–early Holocene transition. Quat. Sci. Rev. 29, 3442–3456. https://doi.org/10.1016/j.quascirev.2010.08.014.

Aarflot, J.M., Skjoldal, H.R., Dalpadado, P., Skern-Mauritzen, M., 2017. Contribution of *Calanus* species to the mesozooplankton biomass in the Barents Sea. ICES J. Mar. Sci. 75, 2342–2354. https://doi.org/10.1093/icesjms/fsx221.

Adkins, J.F., Ingersoll, A.P., Pasquero, C., 2005. Rapid climate change and conditional instability of the glacial deep ocean from the thermobaric effect and geothermal heating. Quat. Sci. Rev. 24, 581–594. https://doi.org/10.1016/j.quascirev.2004.11.005.

Andreassen, K., Winsborrow, M., 2009. Signature of ice streaming in Bjørnøyrenna, polar North Atlantic, through the Pleistocene and implications for ice-stream dynamics. Ann. Glaciol. 50, 17–27. https://doi.org/10.3189/172756409789624238.

Arrigo, K.R., van Dijken, G.L., 2015. Continued increases in Arctic Ocean primary production. Prog. Oceanogr. 136, 60–70. https://doi.org/10.1016/j.pocean.2015.05.002.

Årthun, M., Eldevik, T., Smedsrud, L.H., Skagseth, Ø., Ingvaldsen, R.B., 2012. Quantifying the influence of Atlantic heat on Barents Sea ice variability and retreat. J. Clim. 25, 4736–4743. https://doi.org/10.1175/jcli-d-11-00466.1.

Assmy, P., Fernández-Méndez, M., Duarte, P., Meyer, A., Randelhoff, A., Mundy, C.J., Olsen, L.M., Kauko, H.M., Bailey, A., Chierici, M., Cohen, L., Doulgeris, A.P., Ehn, J.K., Fransson, A., Gerland, S., Hop, H., Hudson, S.R., Hughes, N., Itkin, P., Johnsen, G., King, J.A., Koch, B.P., Koenig, Z., Kwasniewski, S., Laney, S.R., Nicolaus, M., Pavlov, A.K., Polashenski, C.M., Provost, C., Rösel, A., Sandbu, M., Spreen, G., Smedsrud, L.H., Sundfjord, A., Taskjelle, T., Tatarek, A., Wiktor, J., Wagner, P.M., Wold, A., Steen, H., Granskog, M.A., 2017. Leads in Arctic pack ice enable early phytoplankton blooms below snow-covered sea ice. Sci. Rep. 7 article 40850. https://doi.org/10.1038/srep40850.

Bauch, H.A., Erlenkeusser, H., Spielhagen, R.F., Struck, U., Matthiessen, J., Thiede, J., Heinemeier, J., 2001. A multiproxy reconstruction of the evolution of deep and surface waters in the subarctic Nordic seas over the last 30,000 yr. Quat. Sci. Rev. 20, 659–678. https://doi.org/10.1016/S0277-3791(00)00098-6.

Belt, S.T., 2018. Source-specific biomarkers as proxies for Arctic and Antarctic sea ice. Org. Geochem. 125, 277–298. https://doi.org/10.1016/j.orggeochem.2018.10.002.

Belt, S.T., Allard, W.G., Massé, G., Robert, J.-M., Rowland, S.J., 2000. Highly branched isoprenoids (HBIs): identification of the most common and abundant sedimentary isomers. Geochem. Cosmochim. Acta 64, 3839–3851. https://doi.org/10.1016/S0016-7037(00)00464-6.

Belt, S.T., Brown, T.A., Ringrose, A.E., Cabedo-Sanz, P., Mundy, C.J., Gosselin, M., Poulin, M., 2013. Quantitative measurement of the sea ice diatom biomarker IP_{25} and sterols in Arctic sea ice and underlying sediments: further considerations for palaeo sea ice reconstruction. Org. Geochem. 62, 33–45. https://doi.org/10.1016/j.orggeochem.2013.07.002.

Belt, S.T., Brown, T.A., Rodriguez, A.N., Sanz, P.C., Tonkin, A., Ingle, R., 2012. A reproducible method for the extraction, identification and quantification of the Arctic sea ice proxy IP_{25} from marine sediments. Anal. Meth. 4, 705–713. https://doi.org/10.1039/C2AY05728J.

Belt, S.T., Brown, T.A., Smik, L., Assmy, P., Mundy, C.J., 2018. Sterol identification in floating Arctic sea ice algal aggregates and the Antarctic sea ice diatom *Berkeleya adeliensis*. Org. Geochem. 118, 1–3. https://doi.org/10.1016/j.orggeochem.2018.01.008.

Belt, S.T., Brown, T.A., Smik, L., Tatarek, A., Wiktor, J., Stowasser, G., Assmy, P., Allen, C.S., Husum, K., 2017. Identification of C_{25} highly branched isoprenoid (HBI) alkenes in diatoms of the genus *Rhizosolenia* in polar and sub-polar marine phytoplankton. Org. Geochem. 110, 65–72. https://doi.org/10.1016/j.orggeochem.2017.05.007.

Belt, S.T., Cabedo-Sanz, P., Smik, L., Navarro-Rodriguez, A., Berben, S.M.P., Knies, J., Husum, K., 2015. Identification of paleo Arctic winter sea ice limits and the marginal ice zone: optimised biomarker-based reconstructions of late Quaternary Arctic sea ice. Earth Planet. Sci. Lett. 431, 127–139. https://doi.org/10.1016/j.epsl.2015.09.020.

Belt, S.T., Massé, G., Rowland, S.J., Poulin, M., Michel, C., LeBlanc, B., 2007. A novel chemical fossil of palaeo sea ice: IP_{25}. Org. Geochem. 38, 16–27. https://doi.org/10.1016/j.orggeochem.2006.09.013.

Belt, S.T., Müller, J., 2013. The Arctic sea ice biomarker IP_{25}: a review of current understanding, recommendations for future research and applications in palaeo sea ice reconstructions. Quat. Sci. Rev. 79, 9–25. https://doi.org/10.1016/j.quascirev.2012.12.001.

Berben, S.M.P., Husum, K., Navarro-Rodriguez, A., Belt, S.T., Aagaard-Sørensen, S., 2017. Semi-quantitative reconstruction of early to late Holocene spring and summer sea ice conditions in the northern Barents Sea. J. Quat. Sci. 32, 587–603. https://doi.org/10.1002/jqs.2953.

Berger, A., Loutre, M.F., 1991. Insolation values for the climate of the last 10 million years. Quat. Sci. Rev. 10, 297–317. https://doi.org/10.1016/0277-3791(91)90033-Q.

Berger, W.H., Jansen, E., 1995. Younger Dryas episode: ice collapse and superfjord heat pump. In: Troelstra, S.R., van Hinte, J.E., Ganssen, G.M. (Eds.), The Younger Dryas. North-Holland, Amsterdam, Holland, pp. 61–105.

Bjarnadóttir, L.R., Winsborrow, M.C.M., Andreassen, K., 2014. Deglaciation of the central Barents Sea. Quat. Sci. Rev. 92, 208–226. https://doi.org/10.1016/j.quascirev.2013.09.012.

Blaauw, M., Christen, J.A., 2011. Flexible paleoclimate age-depth models using an autoregressive gamma Process. Bayesian Anal. 6, 457–474. https://doi.org/10.1214/11-BA618.

Boetius, A., Albrecht, S., Bakker, K., Bienhold, C., Felden, J., Fernández-Méndez, M., Hendricks, S., Katlein, C., Lalande, C., Krumpen, T., Nicolaus, M., Peeken, I., Rabe, B., Rogacheva, A., Rybakova, E., Somavilla, R., Wenzhöfer, F., 2013. Export of algal biomass from the melting Arctic sea ice. Science 339, 1430–1432. https://doi.org/10.1126/science.1231346.

Boon, J.J., Rijpstra, W.I.C., De Lange, F., De Leeuw, J.W., Yoshioka, M., Shimizu, Y., 1979. Black Sea sterol — a molecular fossil for dinoflagellate blooms. Nature 277, 125–127. https://doi.org/10.1038/277125a0.

Brown, T.A., Belt, S.T., Cabedo-Sanz, P., 2014a. Identification of a novel diunsaturated C_{25} highly branched isoprenoid in the marine tube-dwelling diatom Berkeleya rutilans. Environ. Chem. Lett. 12, 455–460. https://doi.org/10.1007/s10311-014-0472-4.

Brown, T.A., Belt, S.T., Philippe, B., Mundy, C.J., Massé, G., Poulin, M., Gosselin, M., 2011. Temporal and vertical variations of lipid biomarkers during a bottom ice diatom bloom in the Canadian Beaufort Sea: further evidence for the use of the IP_{25} biomarker as a proxy for spring Arctic sea ice. Polar Biol. 34, 1857–1868. https://doi.org/10.1007/s00300-010-0942-5.

Brown, T.A., Belt, S.T., Tatarek, A., Mundy, C.J., 2014b. Source identification of the Arctic sea ice proxy IP_{25}. Nat. Commun. 5 article 4197. https://doi.org/10.1038/ncomms5197.

Cabedo-Sanz, P., Belt, S.T., Knies, J., Husum, K., 2013. Identification of contrasting seasonal sea ice conditions during the Younger Dryas. Quat. Sci. Rev. 79, 74–86. https://doi.org/10.1016/j.quascirev.2012.10.028.

Chauhan, T., Rasmussen, T.L., Noormets, R., 2016. Palaeoceanography of the Barents Sea continental margin, north of Nordaustlandet, Svalbard, during the last 74 ka. Boreas 45, 76–99. https://doi.org/10.1111/bor.12135.

Clark, P.U., Dyke, A.S., Shakun, J.D., Carlson, A.E., Clark, J., Wohlfarth, B., Mitrovica, J.X., Hostetler, S.W., McCabe, A.M., 2009. The Last Glacial Maximum. Science 325, 710–714. https://doi.org/10.1126/science.1172873.

Combaut, G., 1986. GC-MS of plant sterol analysis. In: Linskens, H.F., Jackson, J.F. (Eds.), Gas Chromatography/Mass Spectrometry. Springer Berlin Heidelberg, Berlin, Heidelberg, Germany, pp. 121–133.

Cronin, T.M., Dwyer, G.S., Farmer, J., Bauch, H.A., Spielhagen, R.F., Jakobsson, M., Nilsson, J., Briggs Jr., W.M., Stepanova, A., 2012. Deep Arctic Ocean warming during the last glacial cycle. Nat. Geosci. 5, 631–634. https://doi.org/10.1038/ngeo1557.

De Vernal, A., Gersonde, R., Goosse, H., Seidenkrantz, M.-S., Wolff, E.W., 2013. Sea ice in the paleoclimate system: the challenge of reconstructing sea ice from proxies – an introduction. Quat. Sci. Rev. 78, 1–8. https://doi.org/10.1016/j.quascirev.2013.08.009.

Dokken, T.M., Hald, M., 1996. Rapid climatic shifts during isotope stages 2–4 in the Polar North Atlantic. Geology 24, 599–602. https://doi.org/10.1130/0091-7613(1996)024%3c0599:RCSDIS%3e2.3.CO;2.

Dokken, T.M., Jansen, E., 1999. Rapid changes in the mechanism of ocean convection during the last glacial period. Nature 401, 458–461. https://doi.org/10.1038/46753.

Elverhøi, A., Andersen, E.S., Dokken, T., Hebbeln, D., Spielhagen, R., Svendsen, J.I., Sørlflaten, M., Rørnes, A., Hald, M., Forsberg, C.F., 1995. The growth and decay of the late Weichselian ice sheet in western svalbard and adjacent areas based on Provenance studies of marine sediments. Quat. Res. 44, 303–316. https://doi.org/10.1006/qres.1995.1076.

Eriksen, E., Skjoldal, H.R., Gjøsæter, H., Primicerio, R., 2017. Spatial and temporal changes in the Barents Sea pelagic compartment during the recent warming. Prog. Oceanogr. 151, 206–226. https://doi.org/10.1016/j.pocean.2016.12.009.

Falk-Petersen, S., Hop, H., Budgell, W.P., Hegseth, E.N., Korsnes, R., Løyning, T.B., Børre Ørbæk, J., Kawamura, T., Shirasawa, K., 2000. Physical and ecological processes in the marginal ice zone of the northern Barents Sea during the summer melt period. J. Mar. Syst. 27, 131–159. https://doi.org/10.1016/S0924-7963(00)00064-6.

Falk-Petersen, S., Sargent, J.R., Henderson, J., Hegseth, E.N., Hop, H., Okolodkov, Y.B., 1998. Lipids and fatty acids in ice algae and phytoplankton from the marginal ice zone in the Barents Sea. Polar Biol. 20, 41–47. https://doi.org/10.1007/s003000050274.

Fetterer, F., Knowles, K., Meier, W., Savoie, M., Windnagel, A.K., 2017. Sea Ice Index. NSIDC: National Snow and Ice Data Center, Boulder, Colorado, USA updated daily. https://doi.org/10.7265/N5K072F8. (Accessed 9 April 2019).

Gherardi, J.-M., Labeyrie, L., Nave, S., Francois, R., McManus, J.F., Cortijo, E., 2009. Glacial-interglacial circulation changes inferred from $^{231}Pa/^{230}Th$ sedimentary record in the North Atlantic region. Paleoceanography 24 article PA2204. https://doi.org/10.1029/2008PA001696.

Goad, L.J., 1981. Sterol biosynthesis and metabolism in marine invertebrates. Pure Appl. Chem. 51, 837–852. https://doi.org/10.1351/pac198153040837.

Gosselin, M., Levasseur, M., Wheeler, P.A., Horner, R.A., Booth, B.C., 1997. New measurements of phytoplankton and ice algal production in the Arctic Ocean. Deep Sea Res. Part II Top. Stud. Oceanogr. 44, 1623–1644. https://doi.org/10.1016/S0967-0645(97)00054-4.

Hamm, C., Reigstad, M., Riser, C.W., Mühlebach, A., Wassmann, P., 2001. On the trophic fate of *Phaeocystis pouchetii*. VII. Sterols and fatty acids reveal sedimentation of *P. pouchetii*-derived organic matter via krill fecal strings. Mar. Ecol. Prog. Ser. 209, 55–69. https://doi.org/10.3354/meps209055.

Hassett, R.P., Crockett, E.L., 2009. Habitat temperature is an important determinant of cholesterol contents in copepods. J. Exp. Biol. 212, 71–77. https://doi.org/10.1242/jeb.020552.

Hebbeln, D., Dokken, T., Andersen, E.S., Hald, M., Elverhøi, A., 1994. Moisture supply to northern ice-sheet growth during the Last Glacial Maximum. Nature 370, 357–360. https://doi.org/10.1038/370357a0.

Hegseth, E.N., Sundfjord, A., 2008. Intrusion and blooming of Atlantic phytoplankton species in the high Arctic. J. Mar. Syst. 74, 108–119. https://doi.org/10.1016/j.jmarsys.2007.11.011.

Henderson, R.J., Hegseth, E.N., Park, M.T., 1998. Seasonal variation in lipid and fatty acid composition of ice algae from the Barents Sea. Polar Biol. 20, 48–55. https://doi.org/10.1007/s003000050275.

Hoff, U., Rasmussen, T.L., Stein, R., Ezat, M.M., Fahl, K., 2016. Sea ice and millennial-scale climate variability in the Nordic seas 90 kyr ago to present. Nat. Commun. 7 article 12247. https://doi.org/10.1038/ncomms12247.

Hoppe, C.J.M., Flintrop, C.M., Rost, B., 2018. The Arctic picoeukaryote Micromonas pusilla benefits synergistically from warming and ocean acidification. Biogeosciences 15, 4353–4365. https://doi.org/10.5194/bg-15-4353-2018.

Hormes, A., Gjermundsen, E.F., Rasmussen, T.L., 2013. From mountain top to the deep sea – deglaciation in 4D of the northwestern Barents Sea ice sheet. Quat. Sci. Rev. 75, 78–99. https://doi.org/10.1016/j.quascirev.2013.04.009.

Huang, W.Y., Meinschein, W.G., 1976. Sterols as source indicators of organic materials in sediments. Geochem. Cosmochim. Acta 40, 323–330. https://doi.org/10.1016/0016-7037(76)90210-6.

Hughes, A.L.C., Gyllencreutz, R., Lohne, Ø.S., Mangerud, J., Svendsen, J.I., 2016. The last Eurasian ice sheets – a chronological database and time-slice reconstruction, DATED-1. Boreas 45, 1–45. https://doi.org/10.1111/bor.12142.

Hulbe, C., 2017. Is ice sheet collapse in West Antarctica unstoppable? Science 356, 910–911. https://doi.org/10.1126/science.aam9728.

Ivanov, V.V., Alexeev, V.A., Repina, I., Koldunov, N.V., Smirnov, A., 2012. Tracing Atlantic water signature in the Arctic sea ice cover east of svalbard. Adv. Meteorol. **2012** article 201818. https://doi.org/10.1155/2012/201818.

James, N.A., Matteson, D.S., 2013. Ecp: an R package for nonparametric multiple change point Analysis of multivariate data. J. Stat. Softw. 62, 1–25. https://doi.org/10.18637/jss.v062.i07.

Jennings, A.E., Andrews, J.T., Ó Cofaigh, C., St-Onge, G., Belt, S., Cabedo-Sanz, P., Pearce, C., Hillaire-Marcel, C., Calvin Campbell, D., 2018. Baffin Bay paleoenvironments in the LGM and HS1: resolving the ice-shelf question. Mar. Geol. 402, 5–16. https://doi.org/10.1016/j.margeo.2017.09.002.

Jessen, S.P., Rasmussen, T.L., Nielsen, T., Solheim, A., 2010. A new Late Weichselian and Holocene marine chronology for the western Svalbard slope 30,000–0 cal years BP. Quat. Sci. Rev. 29, 1301–1312. https://doi.org/10.1016/j.quascirev.2010.02.020.

Joseph, L., Villareal, T.A., Lipschultz, F., 1997. A high sensitivity nitrate reductase assay and its application to vertically migrating *Rhizosolenia* mats. Aquat. Microb. Ecol. 12, 95–104. https://doi.org/10.3354/ame012095.

Knies, J., 2005. Climate-induced changes in sedimentary regimes for organic matter supply on the continental shelf off northern Norway. Geochem. Cosmochim. Acta 69, 4631–4647. https://doi.org/10.1016/j.gca.2005.05.014.

Knies, J., Kleiber, H.-P., Matthiessen, J., Müller, C., Nowaczyk, N., 2001. Marine ice-rafted debris records constrain maximum extent of Saalian and Weichselian ice-sheets along the northern Eurasian margin. Glob. Planet. Chang. 31, 45–64. https://doi.org/10.1016/S0921-8181(01)00112-6.

Knies, J., Köseoğlu, D., Rise, L., Baeten, N., Bellec, V.K., Bøe, R., Klug, M., Panieri, G., Jernas, P.E., Belt, S.T., 2018. Nordic Seas polynyas and their role in preconditioning marine productivity during the Last Glacial Maximum. Nat. Commun. 9 article 3959. https://doi.org/10.1038/s41467-018-06252-8.

Knies, J., Stein, R., 1998. New aspects of organic carbon deposition and its paleoceanographic implications along the northern Barents Sea margin during the last 30,000 years. Paleoceanography 13, 384–394. https://doi.org/10.1029/98PA01501.

Knies, J., Vogt, C., Stein, R., 1999. Late Quaternary growth and decay of the Svalbard/Barents Sea ice sheet and paleoceanographic evolution in the adjacent Arctic Ocean. Geo Mar. Lett. 18, 195–202. https://doi.org/10.1007/s003670050068.

Koç, N., Klitgaard-Kristensen, D., Hasle, K., Forsberg, C.F., Solheim, A., 2002. Late glacial palaeoceanography of Hinlopen strait, northern Svalbard. Polar Res. 21, 307–314. https://doi.org/10.3402/polar.v21i2.6492.

Köseoğlu, D., Belt, S.T., Husum, K., Knies, J., 2018b. An assessment of biomarker-based multivariate classification methods versus the PIP_{25} index for paleo Arctic sea ice reconstruction. Org. Geochem. 125, 82–94. https://doi.org/10.1016/j.orggeochem.2018.08.014.

Köseoğlu, D., Belt, S.T., Smik, L., Yao, H., Panieri, G., Knies, J., 2018a. Complementary biomarker-based methods for characterising Arctic sea ice conditions: a case study comparison between multivariate analysis and the PIP_{25} index. Geochem. Cosmochim. Acta 222, 406–420. https://doi.org/10.1016/j.gca.2017.11.001.

Kremer, A., Stein, R., Fahl, K., Bauch, H., Mackensen, A., Niessen, F., 2018a. A 190-ka biomarker record revealing interactions between sea ice, Atlantic Water inflow and ice sheet activity in eastern Fram Strait. Arktos 4 article 22. https://doi.org/10.1007/s41063-018-0052-0.

Kremer, A., Stein, R., Fahl, K., Ji, Z., Yang, Z., Wiers, S., Matthiessen, J., Forwick, M., Löwemark, L., O'Regan, M., Chen, J., Snowball, I., 2018b. Changes in sea ice cover and ice sheet extent at the Yermak Plateau during the last 160 ka – reconstructions from biomarker records. Quat. Sci. Rev. 182, 93–108. https://doi.org/10.1016/j.quascirev.2017.12.016.

Kvile, K.Ø., Langangen, Ø., Prokopchuk, I., Stenseth, N.C., Stige, L.C., 2016. Disentangling the mechanisms behind climate effects on zooplankton. Proc. Natl. Acad. Sci. 113, 1841–1846. https://doi.org/10.1073/pnas.1525130113.

Laskar, J., Robutel, P., Joutel, F., Gastineau, M., Correia, A.C.M., Levrard, B., 2004. A long-term numerical solution for the insolation quantities of the Earth. Astron. Astrophys. 428, 261–285. https://doi.org/10.1051/0004-6361:20041335.

Leblanc, K., Arístegui, J., Armand, L., Assmy, P., Beker, B., Bode, A., Breton, E., Cornet, V., Gibson, J., Gosselin, M.-P., Kopczynska, E.E., Marshall, H., Peloquin, J., Piontkovski, S., Poulton, A.J., Queguiner, B., Schiebel, R., Shipe, R., Stefels, J., van Leeuwe, M.A., Varela, M., Widdicombe, C., Yallop, M., 2012. A global diatom database – abundance, biovolume and biomass in the world ocean. Earth Syst. Sci. Data 4, 149–165. https://doi.org/10.5194/essd-4-149-2012.

Lindsay, R., Schweiger, A., 2015. Arctic sea ice thickness loss determined using subsurface, aircraft, and satellite observations. Cryosphere 9, 269–283. https://doi.org/10.5194/tc-9-269-2015.

Liu, Z., Otto-Bliesner, B.L., He, F., Brady, E.C., Tomas, R., Clark, P.U., Carlson, A.E., Lynch-Stieglitz, J., Curry, W., Brook, E., Erickson, D., Jacob, R., Kutzbach, J., Cheng, J., 2009. Transient simulation of last deglaciation with a new mechanism for Bølling-Allerød warming. Science 325, 310–314. https://doi.org/10.1126/science.1171041.

Loeng, H., 1991. Features of the physical oceanographic conditions of the Barents Sea. Polar Res. 10, 5–18. https://doi.org/10.3402/polar.v10i1.6723.

Marcott, S.A., Clark, P.U., Padman, L., Klinkhammer, G.P., Springer, S.R., Liu, Z., Otto-Bliesner, B.L., Carlson, A.E., Ungerer, A., Padman, J., He, F., Cheng, J., Schmittner, A., 2011. Ice-shelf collapse from subsurface warming as a trigger for Heinrich events. Proc. Natl. Acad. Sci. 108, 13415–13419. https://doi.org/10.1073/pnas.1104772108.

Martin-Creuzburg, D., von Elert, E., 2009. Ecological significance of sterols in aquatic food webs. In: Kainz, M., Brett, M.T., Arts, M.T. (Eds.), Lipids in Aquatic Ecosystems. Springer New York, New York, USA, pp. 43–64. https://doi.org/10.1007/978-0-387-89366-2_3.

McManus, J.F., Francois, R., Gherardi, J.M., Keigwin, L.D., Brown-Leger, S., 2004.

Collapse and rapid resumption of Atlantic meridional circulation linked to deglacial climate changes. Nature 428, 834–837. https://doi.org/10.1038/nature02494.
Mühlebach, A., Albers, C., Kattner, G., 1999. Differences in the sterol composition of dominant antarctic zooplankton. Lipids 34, 45–51. https://doi.org/10.1007/s11745-999-336-1.
Müller, J., Massé, G., Stein, R., Belt, S.T., 2009. Variability of sea-ice conditions in the Fram Strait over the past 30,000 years. Nat. Geosci. 2, 772–776. https://doi.org/10.1038/ngeo665.
Müller, J., Stein, R., 2014. High-resolution record of late glacial and deglacial sea ice changes in Fram Strait corroborates ice–ocean interactions during abrupt climate shifts. Earth Planet. Sci. Lett. 403, 446–455. https://doi.org/10.1016/j.epsl.2014.07.016.
Müller, J., Wagner, A., Fahl, K., Stein, R., Prange, M., Lohmann, G., 2011. Towards quantitative sea ice reconstructions in the northern North Atlantic: a combined biomarker and numerical modelling approach. Earth Planet. Sci. Lett. 306, 137–148. https://doi.org/10.1016/j.epsl.2011.04.011.
Navarro-Rodriguez, A., Belt, S.T., Knies, J., Brown, T.A., 2013. Mapping recent sea ice conditions in the Barents Sea using the proxy biomarker IP_{25}: implications for palaeo sea ice reconstructions. Quat. Sci. Rev. 79, 26–39. https://doi.org/10.1016/j.quascirev.2012.11.025.
Newton, A.M.W., Huuse, M., 2017. Glacial geomorphology of the central Barents Sea: implications for the dynamic deglaciation of the Barents Sea ice sheet. Mar. Geol. 387, 114–131. https://doi.org/10.1016/j.margeo.2017.04.001.
Nichols, P.D., Palmisano, A.C., Rayner, M.S., Smith, G.A., White, D.C., 1990. Occurrence of novel C_{30} sterols in Antarctic sea-ice diatom communities during a spring bloom. Org. Geochem. 15, 503–508. https://doi.org/10.1016/0146-6380(90)90096-I.
Nørgaard-Pedersen, N., Spielhagen, R.F., Erlenkeuser, H., Grootes, P.M., Heinemeier, J., Knies, J., 2003. Arctic Ocean during the Last Glacial Maximum: Atlantic and polar domains of surface water mass distribution and ice cover. Paleoceanography 18 article 1063. https://doi.org/10.1029/2002PA000781.
Notz, D., Marotzke, J., 2012. Observations reveal external driver for Arctic sea-ice retreat. Geophys. Res. Lett. 39 article L08502. https://doi.org/10.1029/2012GL051094.
Onarheim, I.H., Eldevik, T., Smedsrud, L.H., Stroeve, J.C., 2018. Seasonal and regional manifestation of Arctic sea ice loss. J. Clim. 31, 4917–4932. https://doi.org/10.1175/jcli-d-17-0427.1.
Peltier, W.R., Fairbanks, W.G., 2006. Global glacial ice volume and Last Glacial Maximum duration from an extended Barbados sea level record. Quat. Sci. Rev. 25, 3322–3337. https://doi.org/10.1016/j.quascirev.2006.04.010.
R Core Team, 2018. R: A Language and Environment for Statistical Computing. R Foundation for Statistical Computing, Vienna.
Rampen, S.W., Abbas, B.A., Schouten, S., Sinninghe Damste, J.S., 2010. A comprehensive study of sterols in marine diatoms (Bacillariophyta): implications for their use as tracers for diatom productivity. Limnol. Oceanogr. 55, 91–105. https://doi.org/10.4319/lo.2010.55.1.0091.
Rasmussen, T.L., Thomsen, E., 2004. The role of the North Atlantic Drift in the millennial timescale glacial climate fluctuations. Palaeogeogr. Palaeoclimatol. Palaeoecol. 210, 101–116. https://doi.org/10.1016/j.palaeo.2004.04.005.
Rasmussen, T.L., Thomsen, E., 2008. Warm Atlantic surface water inflow to the Nordic seas 34–10 calibrated ka B.P. Paleoceanography 23 article PA1201. https://doi.org/10.1029/2007PA001453.
Rasmussen, T.L., Thomsen, E., Ślubowska, M.A., Jessen, S., Solheim, A., Koç, N., 2007. Paleoceanographic evolution of the SW Svalbard margin (76°N) since 20,000 ^{14}C yr BP. Quat. Res. 67, 100–114. https://doi.org/10.1016/j.yqres.2006.07.002.
Reimer, P., Bard, E., Bayliss, A., Beck, J., Blackwell, P., Ramsey, C., Van der Plicht, J., 2013. IntCal13 and Marine13 radiocarbon age calibration curves 0–50,000 Years cal BP. Radiocarbon 55, 1869–1887. https://doi.org/10.2458/azu_js_rc.55.16947.
Ringrose, A.E., 2012. Temporal and Vertical Distributions of IP_{25} and Other Lipid Biomarkers in Sea Ice from Resolute Bay, Nunavut, Canada. M.Phil. thesis. University of Plymouth, Plymouth, UK.
Ritz, S.P., Stocker, T.F., Grimalt, J.O., Menviel, L., Timmermann, A., 2013. Estimated strength of the Atlantic overturning circulation during the last deglaciation. Nat. Geosci. 6, 208–212. https://doi.org/10.1038/ngeo1723.
Rontani, J.-F., Belt, S.T., Brown, T.A., Amiraux, R., Gosselin, M., Vaultier, F., Mundy, C.J., 2016. Monitoring abiotic degradation in sinking versus suspended Arctic sea ice algae during a spring ice melt using specific lipid oxidation tracers. Org. Geochem. 98, 82–97. https://doi.org/10.1016/j.orggeochem.2016.05.016.
Rontani, J.-F., Belt, S.T., Brown, T.A., Vaultier, F., Mundy, C.J., 2014a. Sequential photo- and autoxidation of diatom lipids in Arctic sea ice. Org. Geochem. 77, 59–71. https://doi.org/10.1016/j.orggeochem.2014.09.009.
Rontani, J.-F., Belt, S.T., Vaultier, F., Brown, T.A., 2011. Visible light induced photooxidation of highly branched isoprenoid (HBI) alkenes: significant dependence on the number and nature of double bonds. Org. Geochem. 42, 812–822. https://doi.org/10.1016/j.orggeochem.2011.04.013.
Rontani, J.-F., Belt, S.T., Vaultier, F., Brown, T.A., Massé, G., 2014b. Autoxidative and Photooxidative reactivity of highly branched isoprenoid (HBI) alkenes. Lipids 49, 481–494. https://doi.org/10.1007/s11745-014-3891-x.
Rørvik, K.-L., Rasmussen, T.L., Hald, M., Husum, K., 2013. Intermediate water ventilation in the Nordic seas during MIS 2. Geophys. Res. Lett. 40, 1805–1810. https://doi.org/10.1002/grl.50325.
Schmittner, A., 2005. Decline of the marine ecosystem caused by a reduction in the Atlantic overturning circulation. Nature 434, 628–633. https://doi.org/10.1038/nature03476.
Shakun, J.D., Clark, P.U., He, F., Marcott, S.A., Mix, A.C., Liu, Z., Otto-Bliesner, B., Schmittner, A., Bard, E., 2012. Global warming preceded by increasing carbon dioxide concentrations during the last deglaciation. Nature 484, 49–54. https://doi.org/10.1038/nature10915.
Signorini, S.R., McClain, C.R., 2009. Environmental factors controlling the Barents Sea spring-summer phytoplankton blooms. Geophys. Res. Lett. 36 article L10604. https://doi.org/10.1029/2009GL037695.
Smedsrud, L.H., Esau, I., Ingvaldsen, R.B., Eldevik, T., Haugan, P.M., Li, C., Lien, V.S., Olsen, A., Omar, A.M., Otterå, O.H., Risebrobakken, B., Sandø, A.B., Semenov, V.A., Sorokina, S.A., 2013. The role of the Barents Sea in the Arctic climate system. Rev. Geophys. 51, 415–449. https://doi.org/10.1002/rog.20017.
Smedsrud, L.H., Halvorsen, M.H., Stroeve, J.C., Zhang, R., Kloster, K., 2017. Fram Strait sea ice export variability and September Arctic sea ice extent over the last 80 years. Cryosphere 11, 65–79. https://doi.org/10.5194/tc-11-65-2017.
Smedsrud, L.H., Ingvaldsen, R.B., Nilsen, J.E.Ø., Skagseth, Ø., 2010. Heat in the Barents Sea: transport, storage, and surface fluxes. Ocean Sci. 6, 219–234. https://doi.org/10.5194/os-6-219-2010.
Smik, L., Cabedo-Sanz, P., Belt, S.T., 2016. Semi-quantitative estimates of paleo Arctic sea ice concentration based on source-specific highly branched isoprenoid alkenes: a further development of the PIP_{25} index. Org. Geochem. 92, 63–69. https://doi.org/10.1016/j.orggeochem.2015.12.007.
Søreide, J.E., Carroll, M.L., Hop, H., Ambrose, W.G., Hegseth, E.N., Falk-Petersen, S., 2013. Sympagic-pelagic-benthic coupling in Arctic and Atlantic waters around Svalbard revealed by stable isotopic and fatty acid tracers. Mar. Biol. Res. 9, 831–850. https://doi.org/10.1080/17451000.2013.775457.
Stein, R., Fahl, K., 2013. Biomarker proxy shows potential for studying the entire Quaternary Arctic sea ice history. Org. Geochem. 55, 98–102. https://doi.org/10.1016/j.orggeochem.2012.11.005.
Stein, R., Fahl, K., Schade, I., Manerung, A., Wassmuth, S., Niessen, F., Nam, S.-I., 2017. Holocene variability in sea ice cover, primary production, and Pacific-Water inflow and climate change in the Chukchi and East Siberian Seas (Arctic Ocean). J. Quat. Sci. 32, 362–379. https://doi.org/10.1002/jqs.2929.
Strass, V.H., Nöthig, E.-M., 1996. Seasonal shifts in ice edge phytoplankton blooms in the Barents Sea related to the water column stability. Polar Biol. 16, 409–422. https://doi.org/10.1007/bf02390423.
Stroeve, J.C., Markus, T., Boisvert, L., Miller, J., Barrett, A., 2014. Changes in Arctic melt season and implications for sea ice loss. Geophys. Res. Lett. 41, 1216–1225. https://doi.org/10.1002/2013GL058951.
Strong, C., Rigor, I.G., 2013. Arctic marginal ice zone trending wider in summer and narrower in winter. Geophys. Res. Lett. 40, 4864–4868. https://doi.org/10.1002/grl.50928.
Syvertsen, E.E., 1991. Ice algae in the Barents Sea: types of assemblages, origin, fate and role in the ice-edge phytoplankton bloom. Polar Res. 10, 277–288. https://doi.org/10.1111/j.1751-8369.1991.tb00653.x.
Tamelander, T., Reigstad, M., Hop, H., Carroll, M.L., Wassmann, P., 2008. Pelagic and sympagic contribution of organic matter to zooplankton and vertical export in the Barents Sea marginal ice zone. Deep Sea Res. II Top. Studies Oceanogr. 55, 2330–2339. https://doi.org/10.1016/j.dsr2.2008.05.019.
Thiagarajan, N., Subhas, A.V., Southon, J.R., Eiler, J.M., Adkins, J.F., 2014. Abrupt pre-Bølling–Allerød warming and circulation changes in the deep ocean. Nature 511, 75–78. https://doi.org/10.1038/nature13472.
Thornalley, D.J.R., Bauch, H.A., Gebbie, G., Guo, W., Ziegler, M., Bernasconi, S.M., Barker, S., Skinner, L.C., Yu, J., 2015. A warm and poorly ventilated deep Arctic Mediterranean during the last glacial period. Science 349, 706–710. https://doi.org/10.1126/science.aaa9554.
Vare, L.L., Massé, G., Belt, S.T., 2010. A biomarker-based reconstruction of sea ice conditions for the Barents Sea in recent centuries. Holocene 20, 637–643. https://doi.org/10.1177/0959683609355179.
Vogt, C., Knies, J., Spielhagen, R.F., Stein, R., 2001. Detailed mineralogical evidence for two nearly identical glacial/deglacial cycles and Atlantic water advection to the Arctic Ocean during the last 90,000 years. Glob. Planet. Chang. 31, 23–44. https://doi.org/10.1016/S0921-8181(01)00111-4.
Volkman, J., 2003. Sterols in microorganisms. Appl. Microbiol. Biotechnol. 60, 495–506. https://doi.org/10.1007/s00253-002-1172-8.
Volkman, J.K., 1986. A review of sterol markers for marine and terrigenous organic matter. Org. Geochem. 9, 83–99. https://doi.org/10.1016/0146-6380(86)90089-6.
Volkman, J.K., Barrett, S.M., Blackburn, S.I., 1999. Eustigmatophyte microalgae are potential sources of C_{29} sterols, C_{22}–C_{28} *n*-alcohols and C_{28}–C_{32} *n*-alkyl diols in freshwater environments. Org. Geochem. 30, 307–318. https://doi.org/10.1016/S0146-6380(99)00009-1.
Volkman, J.K., Barrett, S.M., Dunstan, G.A., Jeffrey, S.W., 1993. Geochemical significance of the occurrence of dinosterol and other 4-methyl sterols in a marine diatom. Org. Geochem. 20, 7–15. https://doi.org/10.1016/0146-6380(93)90076-N.
Von Quillfeldt, C.H., 2000. Common diatom species in arctic spring blooms: their distribution and abundance. Botanica Marina 43, 499–516. https://doi.org/10.1515/BOT.2000.050.
Walsh, J.E., Fetterer, F., Scott Stewart, J., Chapman, W.L., 2017. A database for depicting Arctic sea ice variations back to 1850. Geogr. Rev. 107, 89–107. https://doi.org/10.1111/j.1931-0846.2016.12195.x.
Wassmann, P., Ratkova, T., Andreassen, I., Vernet, M., Pedersen, G., Rey, F., 1999. Spring bloom development in the marginal ice zone and the central Barents Sea. Mar. Ecol. 20, 321–346. https://doi.org/10.1046/j.1439-0485.1999.2034081.

x.
Wassmann, P., Reigstad, M., Haug, T., Rudels, B., Carroll, M.L., Hop, H., Gabrielsen, G.W., Falk-Petersen, S., Denisenko, S.G., Arashkevich, E., Slagstad, D., Pavlova, O., 2006. Food webs and carbon flux in the Barents Sea. Prog. Oceanogr. 71, 232–287. https://doi.org/10.1016/j.pocean.2006.10.003.
Weinelt, M., Vogelsang, E., Kucera, M., Pflaumann, U., Sarnthein, M., Voelker, A., Erlenkeuser, H., Malmgren, B.A., 2003. Variability of north Atlantic heat transfer during MIS 2. Paleoceanography 18 article 1071. https://doi.org/10.1029/2002PA000772.
Willmes, S., Heinemann, G., 2016. Sea-ice Wintertime lead frequencies and regional characteristics in the Arctic, 2003–2015. Remote Sens. 8 article 4. https://doi.org/10.3390/rs8010004.
Winsborrow, M.C.M., Andreassen, K., Corner, G.D., Laberg, J.S., 2010. Deglaciation of a marine-based ice sheet: late Weichselian palaeo-ice dynamics and retreat in the southern Barents Sea reconstructed from onshore and offshore glacial geomorphology. Quat. Sci. Rev. 29, 424–442. https://doi.org/10.1016/j.quascirev.2009.10.001.
Wollenburg, J.E., Knies, J., Mackensen, A., 2004. High-resolution paleoproductivity fluctuations during the past 24 kyr as indicated by benthic foraminifera in the marginal Arctic Ocean. Palaeogeogr. Palaeoclimatol. Palaeoecol. 204, 209–238. https://doi.org/10.1016/S0031-0182(03)00726-0.
Xiao, X., Fahl, K., Müller, J., Stein, R., 2015. Sea-ice distribution in the modern Arctic Ocean: biomarker records from trans-Arctic Ocean surface sediments. Geochem. Cosmochim. Acta 155, 16–29. https://doi.org/10.1016/j.gca.2015.01.029.
Xiao, X., Fahl, K., Stein, R., 2013. Biomarker distributions in surface sediments from the Kara and Laptev seas (Arctic Ocean): indicators for organic-carbon sources and sea-ice coverage. Quat. Sci. Rev. 79, 40–52. https://doi.org/10.1016/j.quascirev.2012.11.028.
Yoder, J.A., Ackleson, S.G., Barber, R.T., Flament, P., Balch, W.M., 1994. A line in the sea. Nature 371, 689–692. https://doi.org/10.1038/371689a0.
Yokoyama, Y., Lambeck, K., De Deckker, P., Johnston, P., Fifield, L.K., 2000. Timing of the last glacial maximum from observed sea-level minima. Nature 406, 713–716. https://doi.org/10.1038/35021035.
Zamelczyk, K., Rasmussen, T.L., Husum, K., Godtliebsen, F., Hald, M., 2014. Surface water conditions and calcium carbonate preservation in the Fram Strait during marine isotope stage 2, 28.8–15.4 kyr. Paleoceanography 29, 1–12. https://doi.org/10.1002/2012PA002448.